

Continual learning under domain transfer with sparse synaptic bursting

Shawn L. Beaulieu^{a,d,e}, Jeff Clune^{c,f}, and Nick Cheney^{b,d,e}

^ashawn.beaulieu@uvm.edu; ^bncheney@uvm.edu; ^cjclune@gmail.com; ^dDepartment of Computer Science, University of Vermont: Burlington, VT, USA; ^eVermont Complex Systems Center; ^fDepartment of Computer Science, University of British Columbia: Vancouver, BC, Canada

Existing machines are functionally specific tools that were made for easy prediction and control. Tomorrow's machines may be closer to biological systems in their mutability, resilience, and autonomy. But first they must be capable of sequentially learning and retaining new information without being exposed to it arbitrarily often. Past efforts to engineer such systems have sought to build or regulate artificial neural networks using disjoint sets of weights that are uniquely sensitive to specific tasks or inputs. This has not yet enabled continual learning over long sequences of previously unseen data without corrupting existing knowledge—a problem known as catastrophic forgetting. In this paper, we introduce a system that can learn sequentially over previously unseen datasets (ImageNet, CIFAR-100) with little forgetting over time. This is done by controlling the activity of weights in a convolutional neural network on the basis of inputs using top-down regulation generated by a second feed-forward neural network. We find that our method learns continually under domain transfer with sparse bursts of heavy-tailed activity in weights that are recycled across tasks, rather than by maintaining task-specific modules. Sparse synaptic bursting is found to balance activity and suppression such that new functions can be learned without corrupting extant knowledge, thus mirroring the balance of order and disorder in systems at the edge of chaos. This behavior emerges during a prior pre-training (or "meta-learning") phase in which regulated synapses are selectively disinhibited, or grown, from an initial state of uniform suppression through prediction error minimization.

neural networks | catastrophic forgetting | cybernetics

Catastrophic forgetting is the phenomenon wherein an artificial neural network trained over a sequence of inputs loses its ability to perform a function it acquired earlier in the sequence as new information is learned (1, 2). This happens because the network's ability to perform a given function is determined by the values of its synapses. Changes to these values, as a consequence of learning, may corrupt functions that are not robust to perturbation. But resistance to change when existing knowledge is insufficient will result in poor fitness to the tasks at hand.

Forgetting is typically overcome by removing the temporal structure of learning with large batches of randomly ordered inputs that are stored at the programmer's discretion (IID training). This eliminates the problem of forgetting because no class of input is restricted to a single segment of the training sequence. All inputs are equally likely to be seen by the network at any point in time, and so cannot be *forgotten* (2). Alternatively, data can be stored by so-called *generative* networks that are trained IID to produce approximations of their inputs, thereby eliminating the need to store the original dataset (3, 4). Moreover, defective knowledge in the IID setting can always be rectified by ever more optimization, because previously learned inputs can be revisited arbitrarily often (5).

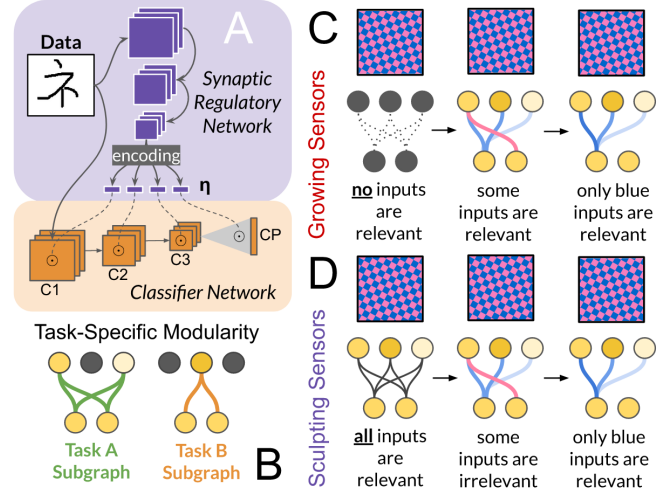


Fig. 1. (A) Model architecture for Tuning Synapses via Allostatic Regulation ("TSAR", Materials and Methods). We refer to regulation of the forward propagation of inputs as synaptic *allostasis* (9) to distinguish it from *homeostatic* modes of regulation, which seek to correct unwanted perturbations (2, 41). **(B)** Task-specific modularity helps to overcome forgetting by maintaining disjoint subgraphs that are each recruited to solve a specific task. This may prevent previously learned functions from being overwritten. **(C)** By initializing meta-learned regulation to be highly suppressant ("Grow", Materials and Methods) we establish a prior on regulation such that no combination of features is relevant to the recruitment of synapses in the classifier. Consequently, the regulator must build sensors by recruiting synapses with initially unspecified functions. Conversely, **(D)** if regulation is initialized to be highly permissive ("Sculpt", Materials and Methods) then *all* inputs are specified as relevant, and meta-learning is the process of making this initial specification more parsimonious. Thus, relevance criteria are autonomously *refined* by sensor sculpting, but autonomously *created* by sensor growth.

But real memories must be actively maintained by the systems that create them, and meaningful participation in the world requires the ability to manage events as they happen in time and space (6–10). Consequently, autonomous systems must be capable of solving the sequential problem of forgetting by their own methods and for their own ends—namely, prediction error minimization.

For neural networks, intelligent behavior is simply what it means to map inputs to outputs in a way that is accurate or useful, but the space of possible actions and percepts usually only changes in light of error (11–20). However, autonomous solutions to problems like catastrophic forgetting require that agents decide for themselves what information is relevant to the tasks they encounter (21–25). This cannot be realized without the freedom to modify the means by which information is created and acquired. For instance: the number of neurons a

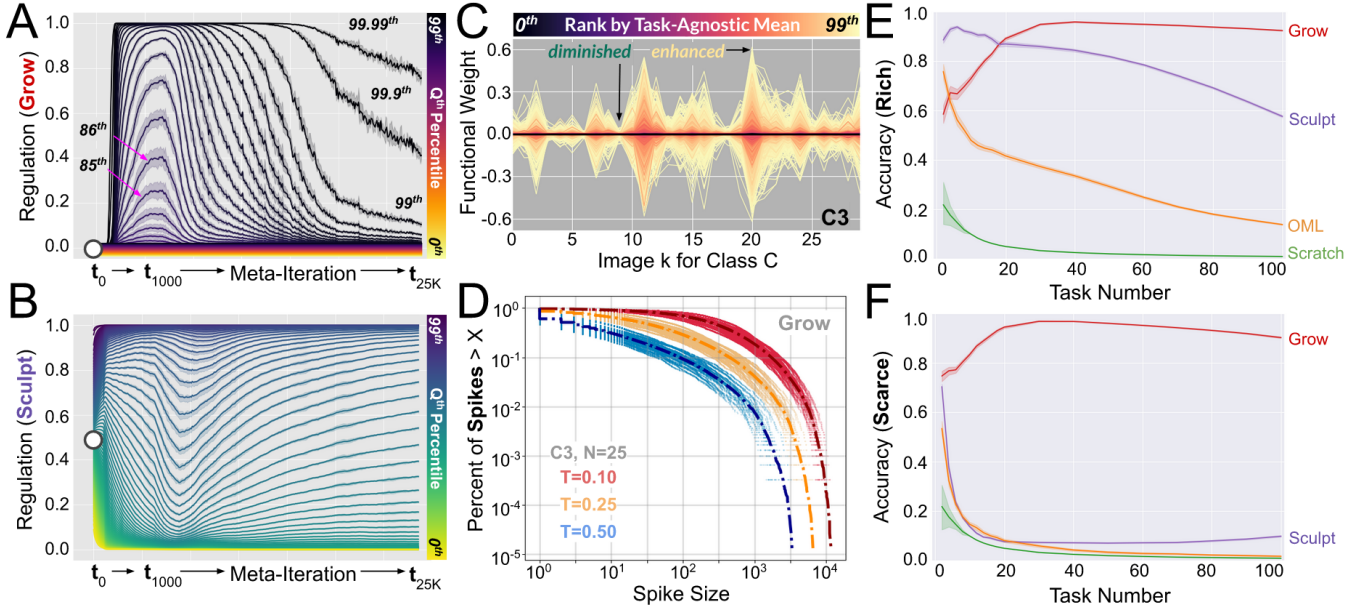


Fig. 2. (A) Meta-learned regulation from an initial state of uniform suppression (*Grow*) results in the rapid deregulation of synapses that are subsequently pruned away as meta-learning proceeds. We plot the Q^{th} percentile of regulation over time measured for 250 randomly sampled meta-learning classes (3750 total inputs). To highlight initial growth, early meta-iterations are plotted with a higher frequency than later meta-iterations. Confidence intervals are computed across runs (lower bound=20th percentile; upper bound=80th percentile). (B) Meta-learned regulation from an initial state of uniform activation (*Sculpt*) results in a bimodal distribution of regulation where the modes are centered on near total suppression and activation, respectively. (C) Regulation in *Grow* under domain transfer to ImageNet produces spikes of *enhanced* and *diminished* activity in the classifier. We plot functional weights in C3 over a single randomly sampled task for a randomly sampled run. Functional weights are defined as synaptic values post-regulatory masking, and are colored by centile according to ranked mean regulation computed over all domain transfer tasks. (D) Increasingly large spikes, which induce greater sensory processing in the classifier, are correspondingly rare. This is shown by plotting the logarithmic complementary cumulative distribution function (54), or CCDF, for which a sub-linear trend obtains for the regulation of all convolutional layers (SI Appendix, Fig.S4, Fig.S5, Fig.S6). Each color represents a different threshold (T) for which a synapse is said to burst if it receives regulation above that threshold, resulting in a binary sequence of length 3000 for each synapse per run (N=25). Individual runs are scatter plotted, while the combined results over all runs are plotted as dash-dot lines. See SI Appendix Fig.S4, Fig.S5, Fig.S6, Fig.S10 for analysis of domain transfer to CIFAR-100 for both data rich and data scarce conditions. (E) ImageNet domain transfer following *data rich* meta-learning (Materials and Methods). Performance curves are generated using 99% bootstrapped confidence intervals (n=1000). **Grow**: Mean=92.2% \pm 1.1% (SD), **Sculpt**: Mean=57.5% \pm 2.8%, **OML**: Mean=13.87% \pm 0.729%, **Scratch**: Mean=0.971% \pm 0.10%. (F) ImageNet domain transfer following *data scarce* meta-learning (Materials and Methods). **Grow**: Mean=90% \pm 2.5% (SD), **Sculpt**: Mean=9.8% \pm 2.9%, **OML**: Mean=1.77% \pm 0.57%, **Scratch**: Mean=0.971% \pm 0.10%.

system possesses, and the manner in which they’re connected, which collectively specify the inputs that can be detected and the actions that can be performed. From this perspective, machine autonomy is about more than the discovery of accurate predictions; it is, among other things, the construction and maintenance of sensors and effectors (11, 26–28).

In this paper we present an algorithm for sequential/continual learning in a convolutional classifier whose synapses are regulated according to the context specified by the present input using a second neural network which itself undergoes continual change. Before learning continually, synaptic regulation is first pre-trained (or “meta-learned”) from an initial state of uniform suppression. This means that no input contains features relevant to the activation of synapses in the classifier. For the system to acquire useful functions, the regulator must learn to *disinhibit* those synapses that maximize prediction accuracy (Fig.1C,D). In so developing functions for initially functionless synapses, the regulator builds sensors for prediction error minimization by establishing “relevance criteria” on inputs not originally specified as relevant (11, 26, 29, 30). As a result, our system becomes more structurally and epistemically autonomous than a traditional neural network, because the information that is detected and optimized by the classifier is expressly a function of regulatory action.

After meta-learning to grow sensors in the classifier, the

system is trained over long sequences of input sampled from previously unseen datasets (*domain transfer*), as regulation itself is greedily optimized. Successful domain transfer then requires the regulator to recruit, adapt, and maintain previously built sensors for continual learning under foreign conditions without succumbing to catastrophic forgetting (or inducing it in the classifier). This differs from past efforts to build systems that learn continually, in which meta-learned neural networks are tested on unseen data from *within* the meta-learning distribution (24, 25) rather than unseen data from *outside* the meta-learning distribution.

Under domain transfer from Omniglot (31) to ImageNet (32) and CIFAR-100 (33), we find that the regulator facilitates continual learning in the classifier by inducing sparse bursts of heavy-tailed activity in weights that are recycled across tasks, rather than by using task-specific modules (2, 24, 25, 34, 35). Sparse synaptic bursting, in which a small cohort of weights is ever active, allows the regulator to control the *amount* of activity in the classifier, rather than its task-modular *location*, such that prior knowledge is protected without blocking adaptation to new inputs. Additionally, we find that bursting synapses are only transiently synchronized, rendering spikes of activity for any given image relatively heterogeneous with respect to past and future spikes. Spike heterogeneity may reflect the creation and storage of robustly distributed memories (?), as the number of unique *subsets* of weights—each of which may

perform a different set of functions—greatly exceeds their total population (36–40). Thus, a given weight may participate in many different functions, but its exclusion from any one of them will negligibly affect the function being computed.

Our analysis suggests that a *balance* of activity and suppression is achieved by regulators set to a specific range of initial meta-learning conditions: when regulation is initialized to be more suppressant or permissive relative to the optimal range, performance under domain transfer falls—often catastrophically. In particular, the emergence of sparse synaptic bursting depends on meta-learning to disinhibit initially suppressed weights (sensor *growth*), rather than by meta-learning to suppress initially disinhibited weights (sensor *sculpting*). Meta-learned sensor growth is characterized by the rapid disinhibition of initially suppressed synapses, followed by a protracted phase of pruning—culminating in a heavy-tailed distribution of synaptic recruitment. This mirrors what has been observed for neural development in biological systems, for which initially sparse connectivity gives way to increased synaptic density in early adolescence, and subsequent pruning of excess connections during teenage and adult years (42, 43). We show that meta-learned sensor growth learns without forgetting under domain transfer even when meta-learning data is reduced to less than 3% of the amount used in prior papers (24, 25).

Tuning synapses via allostatic regulation.

The system we introduce (Fig. 1A, "TSAR") consists of two neural networks: (i) a convolutional classifier network, consisting of three convolutional layers and a linear class prediction layer; and (ii) a feed-forward regulatory network that uses the present input to activate subsets of weights in the classifier for the categorization of that input. Regulation of the forward propagation of inputs also indirectly modulates the degree to which regulated weights are updated in light of error, as was previously demonstrated in the regulation of neurons (25, 35). Given the right sequence of regulation, catastrophic forgetting can then be reduced or eliminated by, for example, partitioning the classifier into task-specific modules (Fig. 1B). Thus, our model has kinship with fast weight memory systems (17, 18, 44, 45) for which information is dynamically routed through a quickly evolving network by a supervising controller that adapts more slowly. However, we do not explicitly encode operations for maintaining a short-term memory, except insofar as previously learned weights are preserved by the regulator.

To maximize control over class predictions, every weight in every layer of the classifier is subject to regulation by multiplicative gating bounded by 0 (completely *inactive*) and 1 (completely *active*). No constraints are placed on when, where, or how much the classifier can learn except those dictated by the regulator in service of prediction error minimization. Therefore our model belongs to the class of continual learning systems that learn how to learn on the basis of empirical success (16, 46–48), rather than by manually designed rules (2, 34, 49–53). As such, we compare our model against other meta-learned algorithms, but reserve claims of intrinsic superiority to different instantiations of TSAR, as our primary concern is the relative advantage conferred by synaptic growth over synaptic sculpting (Section 4).

Meta-learned sensor growth.

In selecting for the ability to learn without forgetting, we first pre-train TSAR using the Online-aware Meta-Learning algorithm (24), or OML. This is a model-agnostic approach to minimizing predictive interference over an outer loop set of previously observed data following an inner loop of sequential updates (Materials and Methods). As a result, our model must meta-learn how to learn over a sequence of images from Omniglot, such that the corresponding updates do not corrupt the ability to classify previously seen Omniglot images. In prior work, this has resulted in the acquisition of task-specific modules (Fig. 1B) through the optimization of neural activations (24, 25). However, the emergence of task-specific modularity as a solution to the OML objective is not required or inevitable. Other solutions, under different conditions, may yet be possible.

In addition to configuring our model for the regulation of *synapses* instead of *neurons* (25), we require that any synapse in the classifier that plays a functional role in class prediction is first “grown” through explicit regulatory action (Fig. 1C,D). This is done by initializing meta-learning with regulation that is highly suppressant. In doing so, we encode a prior on regulation such that no input is relevant to the recruitment of synapses in the classifier. For performant behavior to emerge, the regulator must decide when and where to activate synapses that are otherwise suppressed. Catastrophic forgetting is then evaluated under *domain transfer* by training the meta-learned system on image sequences from previously unseen datasets (Section 5). However, we note that meta-learned synaptic growth is not truly open-ended as in (26), because we manually set both the upper bound on usable synapses and the direction of information flow (e.g. C1 feeds into C2).

Virtual analog to the growth of learning.

Existing algorithms for producing sparse neural networks call upon minimally complex subgraphs within large networks for efficient computation (55–58). This is typically achieved by sculpting away synapses that are unnecessary or that interfere with the supplied objective. By contrast, a wealth of literature attests to the benefits of growing system complexity over time (12–14, 42, 59–62). We hypothesize that one advantage of growth over sculpting is the proximity of the initial state to the least complex (i.e. most sparse) solution, thereby hastening the discovery of “Occam’s Razor” (63). This is particularly important for automating the control of complex systems, as sparse solutions imply the absence of noise and degeneracy, which may amplify causal efficacy (64) and promote the discovery of optimal interventions (65).

For our purposes, regulation can be made to *grow* sensors in the classifier by meta-learning to disinhibit uniformly suppressed synapses, or *sculpted* by meta-learning to suppress uniformly active synapses. We thus obtain Grow and Sculpt regulators by varying the initial strength of regulation to ensure either uniform suppression or activation (Materials and Methods).

All analysis henceforth concerns regulation of the third convolutional layer of the classification network (C3) unless otherwise stated. This is empirically justified by the finding that downstream layers in deep neural networks are the most relevant for understanding performant behavior (66). However, qualitatively identical results were obtained for the regulation

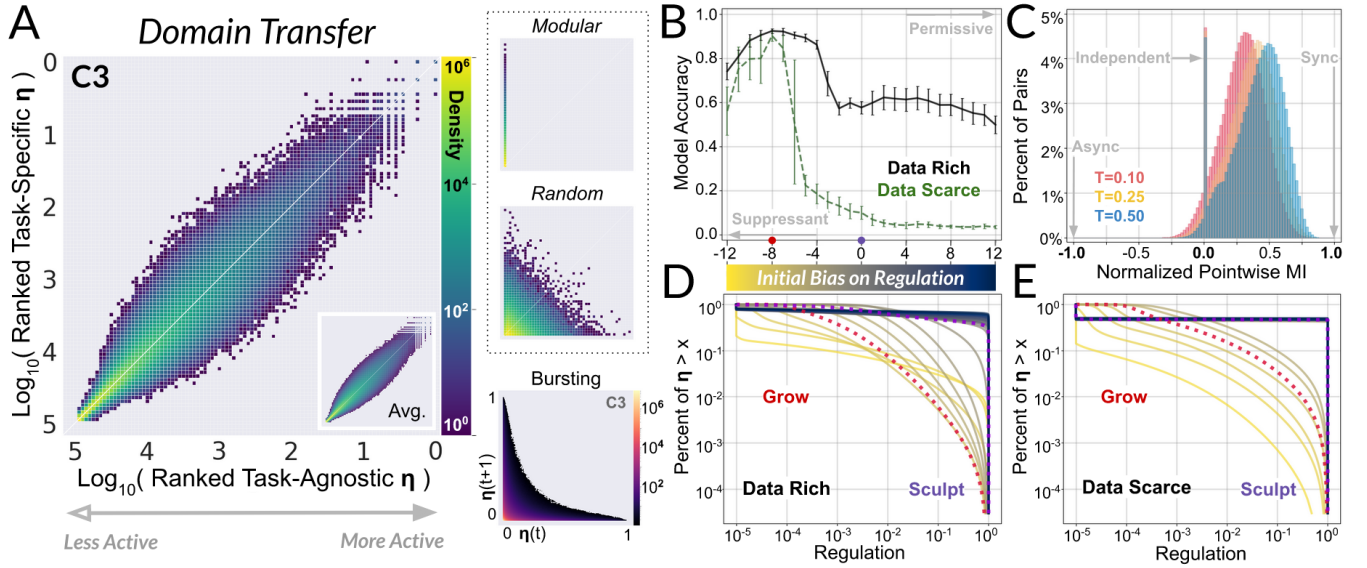


Fig. 3. (A) Regulation under domain transfer does not elicit task-specific modularity. Instead, the most active weights over a given task are the most active weights over all tasks (*synaptic recycling*). For each task, regulatory signals are ranked according to their Task-Specific activity (Eq. 1) and Task-Agnostic activity (Eq. 2). Ranked lists are then transformed to a logarithmic scale (5=least active, 0=most active) and used to fill a two dimensional histogram with 100 bins per dimension (1000 cells in total). The final matrix is filled with data from all 100 tasks for a single run and colored by density on a logarithmic scale (67). The inset reports the average over all runs, with outlier cells of density=1 in less than 25% of runs removed. For individual runs, see SI Appendix Fig.S11 (Rich) and Fig.21 (Scarce). *Synthetic Rankings*: as a conceptual aid, we provide synthetic versions of (A) that report what would be (i) “perfect” task-specific modularity and (ii) Gaussian random regulation. For regulation that is perfectly task *Modular*, weights are randomly sorted into 100 disjoint subsets and assigned (i) a random and constant regulatory signal for the task their subset ID corresponds to, and (ii) a value of 0 for every other task, thus producing synthetic task-specific modules. For regulation that is *Random*, weights are assigned a Gaussian random regulatory signal for all inputs. *Bursting* (non-synthetic): we observe that highly permissive regulation at time t is predictive of suppressant regulation at time $t + 1$. Thus, synaptic recruitment is highly transient (*synaptic bursting*). Time-lagged regulatory outputs under domain transfer are plotted over all runs by stacking two-dimensional histograms for the 75th-99th percentiles of regulation ranked by task-agnostic mean. Lower percentiles are almost uniformly suppressant, and so are omitted from this figure. We then plot the average density over the stack of all runs. Outlier cells that have a density less than or equal to 1 post-stacking are masked. Results for individual runs without masking or stacking are presented in (SI Appendix, Fig.S4). (B) Meta-learned regulation that is initialized to be more permissive (sensor sculpting) is less successful under domain transfer than meta-learned regulation that is initialized to be more suppressant (sensor growth). We report the final performance under domain transfer to ImageNet for the range of meta-learning biases on regulation covering (-12, 12). For each initial bias not equal to 0 (Sculpt) or -8 (Grow), 10 independent models were meta-trained and evaluated under domain transfer over 25 separate runs (250 total runs per treatment). (C) Bursting synapses exhibit a positive bias in their degree of correlation, but very few synapses are strongly synchronized, indicating relatively heterogeneous spike compositions. Each color represents a different threshold (T) for which a synapse is said to burst if it receives regulation above that threshold, resulting in a binary sequence of length 3000 for each synapse per run (N=25). Normalized point-wise mutual information (68) is then computed for each pair of synapses having firing rate > 1% under each threshold for all runs. (D,E) For data rich (D) and data scarce (E) meta-learning, regulators that are increasingly successful under domain transfer generate distributions that are increasingly linear in the logarithmic CCDF. Increasing linearity corresponds to regulation that is increasingly scale-free (54), for which the probability of observing a given regulatory output is inversely proportional to its value. These results show that meta-learned sensor *growth*, but not meta-learned sensor *sculpting*, obtains a *proportional* balance of activity and suppression that is analogous to the balance of order and disorder in critical systems at the edge of chaos (69). We present CCDF plots for the highest performing model for each treatment. Variation between runs is imperceptible, so only a single run per model is plotted. See SI Appendix Fig.S3 for CCDF plots of layers C1 and C2, and Fig.S2 for domain transfer to CIFAR-100.

of upstream convolutional layers (SI Appendix). We reserve analysis of the class prediction layer (CP) for (Section 9), as both the weights and regulation for CP are reset under domain transfer (Materials and Methods).

We find that meta-learning to grow sensors from an initial state of uniform suppression produces highly sparse regulation that follows from the gradual pruning of synapses whose activity rapidly increases at the start of meta-learning (Fig.2A, “Grow”). This process resembles synaptic growth and pruning in developing neurobiological systems (42, 43), and may reflect a learned trade-off between network size and causal efficacy, as larger networks are more powerful but harder to control. Meanwhile, Sculpt meta-learns to suppress synapses that are initially active, but does not produce comparably sparse regulatory output—emitting regulation that is either highly permissive or highly suppressant (Fig.2B). Lower sparsity in Sculpt may be due to the empirical equivalence of sparse and complex models with respect to the OML objective: if increasing sparsity has no impact on performance, or causes it

to diminish, then a gradient toward the most sparse solution does not exist.

However, the logic of meta-learned regulation in either case is not apparent from these facts alone, nor is it obvious whether sensors that have been grown or sculpted by meta-learning can be recruited to learn continually under domain transfer. In the next section we show that meta-learning to grow sensors through purposive deregulation militates against forgetting, while meta-learning to sculpt sensors through suppression does not. After presenting empirical results, we investigate the mechanisms by which forgetting is overcome by meta-learned regulation in Grow (Section 6, Section 7, Section 8).

Domain transfer.

Prior studies test the ability of meta-learned neural networks to avoid catastrophic forgetting on previously unseen data sampled from the same domain used for meta-learning, thereby limiting the extent to which anything new must be learned (25). Instead, we subject our system to input sequences from entirely

new *datasets*. Specifically, we meta-learn on the Omniglot image dataset (31), and test for catastrophic forgetting on input sequences from truncated ImageNet (32) and CIFAR-100 (33). By doing so, we subject our system to a process analogous to the transfer of robots from simulation to reality (70), or the introduction of a novel stressor in biology (71).

Finally, in an effort to move toward true allostatic regulation (9), in which all parameters are in constant flux, we allow the regulatory output layers of TSAR to learn along with the synapses they regulate under domain transfer (Fig.1A, lines emanating from “encoding” vector). This increases susceptibility to forgetting, but allows regulation to adapt to previously unseen input.

Performance.

Fig.2E reports classification accuracy under domain transfer to ImageNet for models trained sequentially over 100 randomly ordered tasks across 250 trials (Materials and Methods). A task is defined as a sequence of 30 randomly sampled instances of a given image class from a set of 600 possible instances, yielding a total of 3,000 sequential gradient updates per trial. Accuracy is measured as the degree to which prior inputs can be recalled. This captures the phenomenon of forgetting by quantifying how much of what was actually learned is remembered over time (24). As stated in the introduction, this problem may be trivially solved in the IID setting, but here we are concerned with the *sequential* problem of forgetting over time. For analysis of generalization accuracy under domain transfer see SI Appendix Fig.S1. To calibrate our understanding of what it means to perform well on this problem, we compare against the meta-learned algorithm, OML (24), as well as the classification network of TSAR without meta-learning or regulation (*Scratch*). However, due to irreconcilable differences in architecture, we cannot meaningfully determine which, if any, algorithm is truly optimal in this context. Thus, we reserve all claims to superiority for different instantiations of TSAR (Fig.3B).

We find that Grow learns sequentially under domain transfer without significant loss in performance as new tasks are encountered, while competing methods adapt sub-optimally or forget catastrophically. To evaluate the robustness of Grow against the degradation of available meta-learning data, we prepared models identical to those presented in Fig.2E but reduced the size of the meta-learning dataset to less than 3% of the original condition (Materials and Methods). We find that the performance of Grow modestly declines relative to the data rich condition, while the other algorithms suffer significant loss in accuracy. Notably, *data scarce* meta-learning in Grow outperforms all other *data rich* models under domain transfer. Similar results obtain for domain transfer to CIFAR-100 with minor variations in accuracy (SI Appendix, Fig.S1). In the next section, we interrogate the means by which TSAR is able to learn continually.

Task-specific modularity.

Past efforts to solve catastrophic forgetting have relied on task-specific modules for conditionally modifying disjoint sets of weights (2, 24, 25, 34). This reduces forgetting because it minimizes the number of times a given weight changes outside its native context. To determine whether regulation in TSAR

is calibrated for such task-specific modularity (Fig.1B), we reason that task-specific modules should be characterized by heightened synaptic activity within a given task but reduced activity for all other tasks. Task-Specific activity for synapse i in layer ℓ is computed as the average regulatory signal governing that synapse, η_i^ℓ , over all K instances of a given task, C (Eq.1). Task-Agnostic activity is computed as the average Task-Specific activity over all tasks not equal to C (Eq.2). In accordance with prior work (55, 56), we take activity to be a proxy for salience, and therefore regard ranked activity as ordered importance. For Grow, regulation is heavy-tailed (Fig.3D,E); as such, we are concerned with *logarithmic* rank (67). Task-specific modularity, or its absence, can then be visualized by plotting ranked Task-Specific activity against ranked Task-Agnostic activity for each task under domain transfer (Fig.3A).

$$\text{Task-Specific Activity} = \frac{1}{K} \sum_{k=0}^K \eta_i^\ell(C_k) \quad [1]$$

$$\text{Task-Agnostic Activity} = \frac{1}{T-1} \sum_{t \neq C} \frac{1}{K} \sum_{k=0}^K \eta_i^\ell(t_k) \quad [2]$$

We find that the synapses which are the most active on a given task are among the most active overall (*synaptic recycling*). Indeed, the majority of weights rank similarly over all tasks as they do for any individual task. Finally, we do not find that any synapse which ranks high for any given task also ranks low for all other tasks. Thus, we do not see evidence for task-specific *modularity* in the output of the regulatory network.

Synaptic bursting.

In the absence of task-specific modularity, we find that synapses are conditionally recruited for task-agnostic bursting (Fig.2C,D, Fig.3A, “Bursting”, SI Appendix Fig.S4). This is characterized by the onset of transient activity in response to particular *images* rather than particular *tasks* (Fig.3A). The simultaneous bursting of multiple synapses generates large *spikes* of activity in weights that are otherwise suppressed. This produces waves of enhanced and diminished processing in the classifier, causing information to be intermittently routed in both the forward propagation of inputs and the back-propagation of error (Fig.2C,D). However, strongly correlated bursting in pairs of synapses across all spikes is rare, indicating variable spike composition (Fig.3C). We note that such transient synchronization may facilitate the creation and storage of robustly distributed memories (?), because previously optimized weights can be recruited to form new coalitions whose function varies with context (36–40). Furthermore, we find that performant regulation under domain transfer exhibits a heavy-tailed distribution, for which the occurrence of regulation that is increasingly large in magnitude is, to a rough approximation, correspondingly improbable (Fig.3B,D,E). Similarly, we find that spikes composed of a given *number* of synapses occur with a probability of inverse proportion (Fig.2D). For these reasons, we claim that performant regulation is calibrated to control the *amount* of sensory processing in the classifier, rather than the task-modular *location* where such processing occurs. This is accomplished

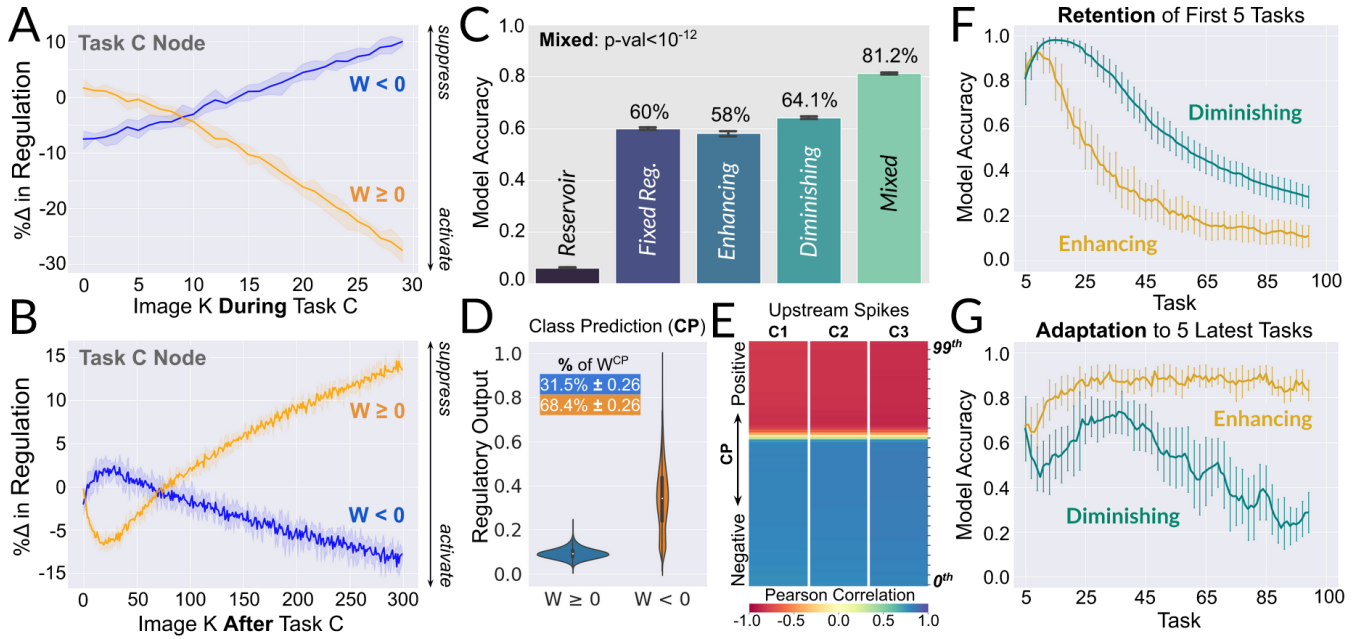


Fig. 4. (A) Task-specific regulation in CP is gradually acquired during training. Over a given task window, negative weights innervating the correct class prediction node are increasingly *suppressed*, while positive weights innervating the correct class node are increasingly *activated*. Percent change is computed over 25 independent runs with respect to mean regulation emitted at the final step of the immediately prior task. (B) Task-specific information is protected when the system is exposed to new tasks. Following a brief refractory period, in which the trends observed in (F) persist over future inputs, positive weights innervating the class prediction nodes of previously seen tasks are increasingly *suppressed* while the negative weights innervating the class prediction nodes of previously seen tasks are *activated*. Percent change is computed over 25 independent runs with respect to mean regulation emitted at the final step of the corresponding task. (C) When a balance of enhanced and diminished perception is artificially induced (*Mixed*) performance greatly exceeds sustained enhancement or diminishment. For “Mixed”, the images that comprise a given task are randomly sampled from the “Enhancing” and “Diminishing” datasets with equal probability. “Fixed” refers to the treatment where regulatory output layers to C1, C2, and C3 is not trainable under domain transfer, showing that successful domain transfer does not merely result from fine-tuning the class prediction layer. “Reservoir” reports model performance for randomly initialized regulation with no meta-learning, showing that meta-learning is needed for successful domain transfer. (D) In the class prediction layer (CP) positive weights are regulated differently than negative weights: positive weights receive regulation that is more suppressant and low variance, while negative weights receive regulation that is more permissive and high variance. This was not observed for convolutional layers. (E) Positive weights in CP are most active when sensory processing in upstream layers is most diminished. During enhanced perception (upstream spikes) negative weights are *activated* and positive weights are *suppressed*. During diminished perception, positive weights are activated and negative weights are suppressed. This is shown by the correlation of upstream spikes with the regulation of negative weights in CP, and the inverse correlation of upstream spikes with the regulation of positive weights in CP. Upstream spikes are defined as the mean regulation for the top 10% of weights in upstream layers ranked by mean regulation over all images. Pearson correlation is computed with respect to (i) the *first difference* for the mean regulation governing weights in CP ranked by weight value and grouped centile; and (ii) the first difference for upstream spikes. We plot the mean Pearson correlation per centile over all 25 models. (F) Sustained enhancement has the effect of corrupting previously acquired functions, while sustained diminishment has the effect of guarding against corruption. (G) Sustained enhancement has the effect of facilitating adaptation to new inputs, while sustained diminishment has the effect of blocking adaptation to new inputs.

by maintaining a proportional balance of activity and suppression—and, thus, a proportional balance of plasticity and stability. Comparatively poor regulation (Sculpt) does not exhibit comparable patterns of regulation.

The proportional balance of contrasting states, like activity/suppression and order/disorder, has previously been implicated in the discovery of optimal communication and memory in simulated networks (72–75), and is believed to play a role in the adaptive behavior of living systems (61, 76). We hypothesize that the initial meta-learning biases on regulation that achieve domain transfer corresponds to a critical range in which regulation learns to balance activity and suppression through meta-learned synaptic growth (Fig.3C,D,E). In this way, our model resolves the tension at the heart of continual learning, in which too much change causes forgetting, while too little change preserves extant functions at the cost of acquiring new ones. Likewise, if the discovery of proportionally balanced activity is critically sensitive to the initial conditions of meta-learned synaptic growth, rather than the precise details of meta-learned data, then fewer inputs may be needed to unlock this function, as illustrated by the success of TSAR

in the data scarce condition (Fig.3B,E). In the next section we investigate the extent to which performance under domain transfer is affected by an even mixture of enhanced and diminished states. Following this, we analyze the regulation of the class prediction layer (CP).

Enhanced and diminished perception.

In order to isolate the effects of enhanced and diminished perception on model performance, we train Grow on sequences of exclusively enhancing or exclusively diminishing images. This is possible because the *mean* regulatory output over all synapses for a given image under domain transfer is virtually identical when the regulatory output layers are trainable compared to when they are fixed (SI Appendix, Fig.S11). Furthermore, analysis of the regulatory network shows that it represents images in a way that is related to their consequent level of overall recruitment, rather than by task identity (SI Appendix, Fig.S5). Thus, in the absence of any learning, we can rank the images for each task on a single axis from maximally-enhancing to maximally-diminishing. *Enhancing* and *Diminishing* datasets are then composed of the top 30

and bottom 30 images per task ranked by mean regulatory output with respect to the model under consideration (out of a possible 600 images per task and 25 independent models of Grow).

When Grow is trained on the Enhancing and Diminishing datasets, performance drops to $58.05\% \pm 3.8\%$ (SD) and $64.1\% \pm 2\%$, respectively (Fig.4C, “Diminishing”, “Enhancing”). However, when the system is trained on an even mixture of enhancing and diminishing images, performance increases relative to both conditions, $81.2\% \pm 1.4\%$ (Fig.4C, “Mixed”: $p\text{-value} < 10^{-12}$, Mann-Whitney U). By visualizing changes in accuracy over time (Fig.4F,G), we find that training on enhancing images degrades retention of past performance but promotes adaptation to new inputs. Conversely, past performance is protected when training on diminishing images, while new inputs become harder to learn. These results further corroborate that our model adapts to novel conditions without corrupting prior functions by maintaining a balance of enhanced and diminished perception (77).

Regulating class predictions.

If upstream sensory processing is characterized by task-agnostic synaptic bursting, how is it that correct class predictions are acquired and maintained by the network? First, we observe that regulation of the class prediction layer (CP) produces markedly different distributions for positive and negative weights (Fig.4D). Positive weights in CP are held at relatively low values with infrequent variation, while negative weights in CP exhibit comparatively high variation around a larger mean value. At the same time, positive and negative weights are differentially correlated with upstream activity, such that negative weights are enhanced and diminished in synchrony with upstream weights, but positive weights are diminished during upstream *enhancement* and enhanced during upstream *diminishment* (Fig.4E). This manner of coordination across layers suggests that different modes of computation are reserved for enhanced and diminished states (77–79).

For instance, positive weights in CP are most active when sensory processing is most diminished (Fig.4E) and, therefore, learn under conditions that are minimally biased by upstream layers. This provides the opportunity to update class predictions independently of how sensory processing was previously optimized. Meanwhile, if we regard the function, if not the purpose, of upstream spiking to be a form of input sampling (77), then the synchronization of negative weights in CP with upstream spikes could be an exploratory mechanism whereby input sampling is coupled with output sampling. Under conditions of uncertainty, with domain transfer being particularly extreme for ANNS, such exploratory maneuvers may be critical for learning. In both cases these properties emerge opportunistically (that is, without foresight) by local prediction error minimization.

In light of these results, we track the average change in regulation governing the positive and negative weights of a given task node, C, over two non-overlapping windows in time: (i) when task C is being learned; and (ii) when the next 10 tasks that follow task C are learned (Fig.4A,B). We find that when task C is learned, the positive weights innervating task node C are gradually *activated*, while the negative weights innervating task node C are gradually *suppressed* (Fig.4A). But when future tasks are encountered this trend is inverted:

positive weights are suppressed while negative weights are activated (Fig.4B). Consequently, we argue that task-specific information for a given task is encoded in the positive weights innervating the corresponding task node. This information is then protected under task-switching with the relative suppression of positive weights in C and the relative activation of negative weights in C. This both protects the information encoded by the weights of task node C, and dampens its excitation when new tasks are encountered. We posit that differential correlation of positive and negative weights in CP with upstream spiking facilitates the emergence of these strategies for regulating class predictions.

Together these results indicate how task-specific predictions are acquired and maintained alongside task-agnostic upstream bursting. However, we find that optimizing the regulation of CP under domain transfer is not, on its own, sufficient to achieve high performance: when regulatory output layers responsible for upstream convolutions are fixed, but regulation of CP is trainable, performance drops relative to the condition where regulatory output for all layers is trainable (Fig.4C, “Fixed”). From this we conclude that optimizing the weights and the regulation for *all layers* is necessary for successful domain transfer, despite increased susceptibility to catastrophic forgetting.

Discussion.

Among the factors responsible for the resilience of living systems is the ability to impose meaning on the world through the negotiation of bodily form and function (11, 26, 27, 80–83). Unlike machine learners, living systems act and perceive in ways that cannot be understood as information transmitted over anatomically fixed, yet tunable, channels (28, 84, 85). Rather, the means by which information is made and transmitted are themselves subject to purposive modification. Thus, encoded in the very structure of living systems is that which counts as meaningful (10, 80, 86–88). By contrast, machine learners typically undergo change only in light of error (56), or by random mutation (16), rendering them partially autonomous systems for error *correction* rather than error *prevention* (9, 41).

In the preceding sections we presented a machine learning algorithm for dynamically regulating synapses in a convolutional neural network for continual learning over sequences of previously unseen datasets. We showed that effective regulation under domain transfer depends on a degree of structural and epistemic autonomy (11, 26) resulting from the adaptive construction of sensors in the classifier. This occurs by meta-learning to disinhibit synapses initialized to a state of uniform suppression, leading to the autonomous construction of relevance criteria on inputs (Fig.1C).

Under domain transfer, we found that regulation does not elicit task-specific modularity, but instead induces sparse bursts of activity in weights that are recycled across tasks. Sparse synaptic bursting is found to be heavy-tailed in both its output (Fig.3D) and in the number of synapses it causes to burst (Fig.3C). We propose that such behavior induces a proportional balance of enhanced and diminished processing in the classifier, thereby enabling adaptation to new inputs without corrupting extant functions. This addresses the core dilemma of continual learning: too much change causes forgetting, while too little change induces brittleness.

Balancing activity and suppression in this way might also

empower optimal communication between layers by managing the *amount* of sensory processing that occurs, rather than its task-modular location (73). Similar dynamics obtain for the phenomenon of ‘virtual governors’ (89, 90) for which emergent relational properties, like temperature and pressure, offer more causally effective targets for intervention than the elements that compose them (64). Analogously, the balance of coarse-grained regulatory states that are insensitive to the precise details of context, like enhanced and diminished perception, could secure greater regulatory efficacy than more fine-grained methods of control. At the same time, component *recycling* is one of the signatures of living systems (85), and has been proposed to distinguish perception as a mediator of *interaction* (36, 37, 91) rather than a system for constructing accurate world models (92). Accordingly, we might not conceptualize inputs as the *cause* of detailed regulatory patterns, but as *occasions* for regulatory action that express the internal laws by which the system maintains its viability (87, 93).

Finally, we presented evidence that task-specific information encoded in the class prediction layer is safely obtained and protected under task-switching by differentially correlating positive and negative weights in CP with task-agnostic upstream spikes (Fig.4A,B).

However, the model we have presented is not particularly sophisticated: the regulator is a simple feed-forward network that lacks both temporal recurrence and bottom-up signaling from the classifier. Therefore, it is blind to the system it regulates, except by way of back-propagation. Moreover, the classifier itself is but a simple convolutional neural network. In part, this is true by necessity, as the size of the regulatory network explodes when the size of the regulated network increases (17). Future work will attempt to grow the complexity of TSAR, and expand the set of problems for which it’s deployed, while mitigating computational explosion with methods like indirect encodings (94). We also believe that TSAR can be combined with existing methods for achieving high generalization accuracy (*offline*) by serving as an adaptable memory that can retain information obtained over long sequences (*online*). Finally, we hope to explore more rigorously the relationship between network growth, synaptic bursting, and heavy-tailed patterns of connectivity, particularly as it applies to the theory and control of morphogenesis in living systems (76, 77, 90, 95–99).

Nevertheless, our findings may be of immediate use in programs for computer vision, reinforcement learning, and robotics. Additionally, our system may be helpful in understanding how information is stored and transmitted in biological systems marked by endless change, stochasticity, opportunism, and multiple functionality (85, 96, 100–102). More abstractly, we believe our work contributes to a growing literature that rejects the supremacy of fixed and fragile automata (103–106). As advances in biology continue to undermine the view that life’s constituent parts are little more than (20th century) machines (28, 85), our technologies should likewise be reconfigured for perpetual and collective modification in response to individual and social preference. The ability to learn new information without forgetting will be critical in the transition to such increasingly protean technology (107).

Materials and Methods

Meta-Learning Algorithm. We use the model-agnostic Online Meta-Learning algorithm (24) for learning how to learn over the background partition of the Omniglot image dataset (31). This dataset contains 963 hand-written character classes taken from various human alphabets. Each character class contains 20 unique instances (15 for training; 5 for testing). All images are resized to 3x28x28 (channels, height, width). A single meta-iteration consists of (i) an inner loop of sequential training on a 20 image batch sampled with replacement from the set of 15 meta-training images for a single character class $c_m \sim \mathcal{C}$; and (ii) an outer loop that evaluates performance retention on a random batch of 84 images sampled from the set of meta-testing images over all classes. Of the 84 images in the performance retention set, 20 are sampled with replacement from the set of 5 meta-testing images from the inner loop class, c_m , while the other 64 images are randomly sampled from the remaining set of 962 character classes.

Prediction error on the performance retention set at the end of the inner loop sequence for network Θ_K^m is back-propagated through the entire model to update the weights used at the beginning of the inner loop sequence, Θ_0^m . These new initial weights are then carried over into the next meta-iteration, $\Theta_0^{m+1} \propto \Theta_0^m + \text{update}$. Learning within each inner loop is discarded: only the initial weights, or the conditions under which inner loop learning occurs, are optimized over the outer loop as per (47). Successful meta-learners will have learned to learn over the inner loop without interfering with the classification of outer loop images, thus directly optimizing for the ability to learn without forgetting or interference (24).

Treatments presented in this paper differ both in their architecture, and in which layers are trainable during inner loop meta-learning. Because of this, we make no claims as to the *inherent* superiority of one model over another. Each treatment, having 25 independent models, was meta-learned for 25,000 meta-iterations on a single NVIDIA Tesla V100 GPU. For more details regarding the meta-learning protocol see (24, 25, 47).

All models will be made available for download. If the reader would like to replicate or extend this work, but lacks the necessary resources, requests for computation can be addressed to the primary author.

Data Rich/Scarce Meta-Learning. Data rich meta-learning uses the full background set of Omniglot images (963 character classes) for the OML protocol. The data scarce condition instead uses less than 3% of the meta-learning data used in the data rich condition (25 randomly sampled character classes).

Domain Transfer. After executing the meta-learning protocol, each model is trained over a sequence of 100 classes from a previously unobserved dataset (ImageNet or CIFAR-100). Classes contain 600 total images, from which 30 are randomly sampled without replacement for each class. This translates to 3000 (100*30) sequential iterations of gradient descent. All images are resized to 3x28x28 (channels, height, width). Every run uses a different random seed, a randomized class order, and a random batch of 30 images per class. We applied a grid search over learning rates, and selected the highest performing setting over all subsequent runs.

OML. See (24, 25) for more details regarding theoretical motivation and network architecture. No changes were made to the meta-learning protocol, except to implement a post-publication correction for computing second-order gradients. The OML treatment, which is distinct from the OML *protocol*, consists of two neural networks: a representation learning network (RLN) composed of five convolutional layers, and a prediction learning network (PLN) composed of two linear layers that takes as input the output of the RLN. During meta-learning, the RLN is updated over the outer loop, while the PLN is updated in both the inner and outer loops. Under domain transfer, the RLN is fixed over the course of training, while the PLN is fully trainable. Prior to domain transfer, the class prediction layer (CP) of the PLN is randomly reset as per (24).

TSAR. TSAR (Fig.1A) consists of two neural networks: a regulatory network, and a classifier network. The regulatory network consists of (i) a perception module; and (ii) a regulatory output layer. The regulatory perception module contains 3 convolutional layers, each containing 192 channels (window size=(3,3), stride=1, padding=0).

The output of each convolutional layer is first processed with instance normalization and then passed through a ReLU non-linear activation function. Max-pooling layers (stride=2, kernel size=2) are placed after the first two convolutional layers of the perception module to create an encoding layer of size 1728 from which all regulatory output is generated (Fig.1A).

The regulatory output layer consists of four weight matrices, each of which produces a set of regulatory outputs that govern a specific layer in the classification network. Raw outputs from the regulatory output layer are passed through a sigmoidal activation before modulating synapses in the classifier via multiplicative gating ($\eta^\ell \odot W^\ell$, for layer ℓ in the classifier).

The classification network is made up of three convolutional layers (112 channels, window size=(3,3), stride=1, padding=0) and a linear output, or class prediction, layer (CP). Max-pooling layers (stride=2, kernel size=2) are placed after each convolutional layer and are followed by instance normalization and a ReLU non-linearity. Class predictions are computed with a softmax function applied to the raw output of the modulated CP layer. During meta-learning, the regulatory network is fixed during inner loop learning, but the prediction network is trainable. All parameters receive updates in the outer loop.

Under domain transfer, all layers in the prediction network are trainable. The regulatory output layer is also trainable. Only the convolutional layers of the regulatory network are fixed. As with OML, the CP layer (and the regulatory output that flows to this layer) is reset before domain transfer.

Grow and Sculpt. For *Grow*, all biases in the regulatory output layer are initialized to a value of -8 before executing the meta-learning protocol. Due to the sigmoidal activation, this results in initially high levels of suppression. For *Sculpt*, all biases in the regulatory output layer are initialized to the standard bias of 0 before executing the meta-learning protocol. Thus, all things being equal, synapses in the classification network of Sculpt begin meta-learning with their functional values approximately halved ($\text{sigmoid}(0.0)=0.5$). Under domain transfer, regulatory output to CP is reset with a bias of -2. This value was obtained using a grid search over CP biases and learning rates on domain transfer accuracy. Regulatory output to CP for Sculpt is reset with the same bias. We found the final performance of Sculpt was insensitive to changes in this value.

Scratch. This treatment uses the classification network architecture described for TSAR, but with regulation disabled. Scratch is subject to domain transfer starting from a random initialization with no meta-learning.

ACKNOWLEDGMENTS. This work is supported in part by the DARPA Lifelong Learning Machines award HR0011-18-2-0018. We'd like to thank Josh C. Bongard, Sam Kriegman, Bryn Loftness, and Kate Nolfi for discussion and proofreading. Computations were performed on the Vermont Advanced Computing, supported in part by NSF award No.OAC-1827314. We also recognize the Vermont Complex Systems Center for assistance, encouragement, and feedback, particularly Lapo Frati and Colin Van Oort.

1. MR French, Catastrophic forgetting in connectionist networks. *Trends Cogn. Sci.* **3**, 128–135 (1999).
2. J Kirkpatrick, et al., Overcoming catastrophic forgetting in neural networks. *Proc. Natl. Acad. Sci.* **114**, 3521–3526 (2017).
3. H Shin, JK Lee, J Kim, J Kim, Continual learning with deep generative replay in *Advances in Neural Information Processing Systems*, eds. I Guyon, et al. (Curran Associates, Inc.), Vol. 30, (2017).
4. GM van de Ven, HT Siegelmann, AS Tollas, Brain-inspired replay for continual learning with artificial neural networks. *Nat. Commun.* **11** (2020).
5. O Vinyals, et al., Grandmaster level in StarCraft II using multi-agent reinforcement learning. *Nature* **575**, 350–354 (2019).
6. F Varela, H Maturana, R Uribe, Autopoiesis: The organization of living systems, its characterization and a model. *Biosystems* **5**, 187–196 (1974).
7. SJ Cooper, From Claude Bernard to Walter Cannon. emergence of the concept of homeostasis. *Appetite* **51**, 419–427 (2008).
8. D Bullock, Adaptive neural models of queuing and timing in fluent action. *Trends Cogn. Sci.* **8**, 426–433 (2004).
9. J Schulkin, P Sterling, Allostasis: A brain-centered, predictive mode of physiological regulation. *Trends Neurosci.* **42**, 740–752 (2019).
10. K Man, A Damasio, Homeostasis and soft robotics in the design of feeling machines. *Nat. Mach. Intell.* **1**, 446–452 (2019).

11. P Cariani, To evolve an ear. epistemological implications of Gordon Pask's electrochemical devices. *Syst. Res.* **10**, 19–33 (2007).
12. J Bongard, Morphological change in machines accelerates the evolution of robust behavior. *Proc. Natl. Acad. Sci.* **108**, 1234–1239 (2011).
13. A Bernatskiy, JC Bongard, Exploiting the relationship between structural modularity and sparsity for faster network evolution in *Proceedings of the Companion Publication of the 2015 Annual Conference on Genetic and Evolutionary Computation*. (ACM), (2015).
14. G Raghavan, M Thomson, Neural networks grown and self-organized by noise in *Advances in Neural Information Processing Systems*, eds. H Wallach, et al. (Curran Associates, Inc.), Vol. 32, (2019).
15. Y Jaafar, J Luc Laurent, A Deruyver, M Saber Naceur, Reinforcement learning for neural architecture search: A review. *Image Vis. Comput.* **89**, 57–66 (2019).
16. KO Stanley, R Miikkulainen, Evolving neural networks through augmenting topologies. *Evol. Comput.* **10**, 99–127 (2002).
17. J Schmidhuber, Learning to control fast-weight memories: An alternative to dynamic recurrent networks. *Neural Comput.* **4**, 131–139 (1992).
18. J Ba, GE Hinton, V Mnih, JZ Leibo, C Ionescu, Using fast weights to attend to the recent past in *Advances in Neural Information Processing Systems*, eds. D Lee, M Sugiyama, U Luxburg, I Guyon, R Garnett. (Curran Associates, Inc.), Vol. 29, (2016).
19. K Greff, S van Steenkiste, J Schmidhuber, On the binding problem in artificial neural networks. *CoRR abs/2012.05208* (2020).
20. I Schlag, K Irie, J Schmidhuber, Linear transformers are secretly fast weight memory systems. *CoRR abs/2102.11174* (2021).
21. AJ Bell, TJ Sejnowski, An information-maximization approach to blind separation and blind deconvolution. *Neural Comput.* **7**, 1129–1159 (1995).
22. K Fukushima, Neocognitron: A hierarchical neural network capable of visual pattern recognition. *Neural Networks* **1**, 119–130 (1988).
23. RL Fry, The engineering of cybernetic systems in *AIP Conference Proceedings*. (AIP), (2002).
24. K Javed, M White, Meta-learning representations for continual learning in *Advances in Neural Information Processing Systems*, eds. H Wallach, et al. (Curran Associates, Inc.), Vol. 32, pp. 1820–1830 (2019).
25. S Beaulieu, et al., Learning to continually learn in *Proceedings of the 24th European Conference on Artificial Intelligence*. (2020).
26. G Pask, The simulation of learning and decision-making behavior in *Aspects of the Theory of Artificial Intelligence*. (Springer US), pp. 165–210 (1962).
27. M Pharoah, Causation and information: Where is biological meaning to be found? *Biosemiotics* **13**, 309–326 (2020).
28. J Bongard, M Levin, Living things are not (20th century) machines: Updating mechanism metaphors in light of the modern science of machine behavior. *Front. Ecol. Evol.* **9** (2021).
29. JM Mandler, How to build a baby: II. conceptual primitives. *Psychol. Rev.* **99**, 587–604 (1992).
30. J Kober, B Mohler, J Peters, Learning perceptual coupling for motor primitives in *2008 IEEE/RSJ International Conference on Intelligent Robots and Systems*. pp. 834–839 (2008).
31. BM Lake, R Salakhutdinov, JB Tenenbaum, Human-level concept learning through probabilistic program induction. *Science* **350**, 1332–1338 (2015).
32. O Russakovsky, et al., ImageNet large scale visual recognition challenge. *Int. J. Comput. Vis.* **115**, 211–252 (2015).
33. A Krizhevsky, G Hinton, Learning multiple layers of features from tiny images. (2009).
34. KO Ellefsen, JB Mouret, J Clune, Neural modularity helps organisms evolve to learn new skills without forgetting old skills. *PLOS Comput. Biol.* **11**, e1004128 (2015).
35. NY Masse, GD Grant, DJ Freedman, Alleviating catastrophic forgetting using context-dependent gating and synaptic stabilization. *Proc. Natl. Acad. Sci.* **115**, E10467–E10475 (2018).
36. M Anderson, *After Phenology: Neural Reuse and the Interactive Brain*. (MIT Press), (2014).
37. J Bruineberg, E Rietveld, What's inside your head once you've figured out what your head's inside of. *Ecol. Psychol.* **31**, 198–217 (2019).
38. W Maass, H Markram, On the computational power of circuits of spiking neurons. *J. Comput. Syst. Sci.* **69**, 593–616 (2004).
39. A Palmigiano, T Geisel, F Wolf, D Battaglia, Flexible information routing by transient synchrony. *Nat. Neurosci.* **20**, 1014–1022 (2017).
40. C Stringer, M Pachitariu, N Steinmetz, M Carandini, KD Harris, High-dimensional geometry of population responses in visual cortex. *Nature* **571**, 361–365 (2019).
41. RC Conant, WR Ashby, Every good regulator of a system must be a model of that system. *Int. J. Syst. Sci.* **1**, 89–97 (1970).
42. U Neniskyte, CT Gross, Errant gardeners: glial-cell-dependent synaptic pruning and neurodevelopmental disorders. *Nat. Rev. Neurosci.* **18**, 658–670 (2017).
43. AP Millán, JJ Torres, S Johnson, J Marro, Concurrence of form and function in developing networks and its role in synaptic pruning. *Nat. Commun.* **9** (2018).
44. WR Ashby, *Design for a brain: The origin of adaptive behaviour (2nd ed. rev.)*. (Chapman & Hall), (1960).
45. B Tsuda, KM Tye, HT Siegelmann, TJ Sejnowski, A modeling framework for adaptive lifelong learning with transfer and savings through gating in the prefrontal cortex. *Proc. Natl. Acad. Sci.* **117**, 29872–29882 (2020).
46. F Zenke, B Poole, S Ganguli, Continual learning through synaptic intelligence in *Proceedings of the 34th International Conference on Machine Learning*, Proceedings of Machine Learning Research, eds. D Precup, YW Teh. (PMLR, International Convention Centre, Sydney, Australia), Vol. 70, pp. 3987–3995 (2017).
47. C Finn, P Abbeel, S Levine, Model-agnostic meta-learning for fast adaptation of deep networks in *Proceedings of the 34th International Conference on Machine Learning*, Proceedings of Machine Learning Research, eds. D Precup, YW Teh. (PMLR, International Convention Centre, Sydney, Australia), Vol. 70, pp. 1126–1135 (2017).
48. H Pham, M Guan, B Zoph, Q Le, J Dean, Efficient neural architecture search via parameters sharing in *Proceedings of the 35th International Conference on Machine Learning*.

- Proceedings of Machine Learning Research, eds. J Dy, A Krause. (PMLR, Stockholmmsässan, Stockholm Sweden), Vol. 80, pp. 4095–4104 (2018).
49. D Isele, A Cosgun, Selective experience replay for lifelong learning. *Proc. AAAI Conf. on Artif. Intell.* **32** (2018).
 50. C Fernando, et al., Pathnet: Evolution channels gradient descent in super neural networks. *ArXiv abs/1701.08734* (2017).
 51. MR French, Semi-distributed representations and catastrophic forgetting in connectionist networks. *Connect. Sci.* **4**, 365–377 (1992).
 52. X Li, Y Grandvalet, F Davoine, Explicit inductive bias for transfer learning with convolutional networks in *Proceedings of the 35th International Conference on Machine Learning*, Proceedings of Machine Learning Research, eds. J Dy, A Krause. (PMLR, Stockholmmsässan, Stockholm Sweden), Vol. 80, pp. 2825–2834 (2018).
 53. J Zhang, et al., Top-down neural attention by excitation backprop. *Int. J. Comput. Vis.* **126**, 1084–1102 (2017).
 54. MPH Stumpf, MA Porter, Critical truths about power laws. *Science* **335**, 665–666 (2012).
 55. Y LeCun, JS Denker, SA Solla, Optimal brain damage in *Advances in Neural Information Processing Systems*. (Morgan Kaufmann), pp. 598–605 (1990).
 56. H Tanaka, D Kunin, DLK Yamins, S Ganguli, Pruning neural networks without any data by iteratively conserving synaptic flow. *CoRR abs/2006.05467* (2020).
 57. U Evcı, YA Ioannou, C Keskin, Y Dauphin, Gradient flow in sparse neural networks and how lottery tickets win (2020).
 58. Y Bengio, N Léonard, AC Courville, Estimating or propagating gradients through stochastic neurons for conditional computation. *ArXiv abs/1308.3432* (2013).
 59. SA Kauffman, Autocatalytic sets of proteins. *J. Theor. Biol.* **119**, 1–24 (1986).
 60. DJ Watts, SH Strogatz, Collective dynamics of ‘small-world’ networks. *Nature* **393**, 440–442 (1998).
 61. O Sporns, DR Chialvo, M Kaiser, CC Hilgetag, Organization, development and function of complex brain networks. *Trends Cogn. Sci.* **8**, 418–425 (2004).
 62. A Gopnik, Childhood as a solution to explore–exploit tensions. *Philos. Transactions Royal Soc. B: Biol. Sci.* **375**, 20190502 (2020).
 63. A Baker, Simplicity in *The Stanford Encyclopedia of Philosophy*, ed. EN Zalta. (Metaphysics Research Lab, Stanford University), Winter 2016 edition, (2016).
 64. EP Hoel, L Albantakis, G Tononi, Quantifying causal emergence shows that macro can beat micro. *Proc. Natl. Acad. Sci.* **110**, 19790–19795 (2013).
 65. J Pearl, *Causality: Models, Reasoning and Inference*. (Cambridge University Press, USA), 2nd edition, (2009).
 66. VV Ramasesh, E Dyer, M Raghu, Anatomy of catastrophic forgetting: Hidden representations and task semantics (2020).
 67. PS Dodds, et al., Allotaxonomy and rank-turbulence divergence: A universal instrument for comparing complex systems (2020).
 68. KW Church, P Hanks, Word association norms, mutual information, and lexicography. *Comput. Linguist.* **16**, 22–29 (1990).
 69. SA Kauffman, S Johnsen, Coevolution to the edge of chaos: Coupled fitness landscapes, poised states, and coevolutionary avalanches. *J. Theor. Biol.* **149**, 467–505 (1991).
 70. JB Mouret, K Chatzilygeroudis, 20 years of reality gap in *Proceedings of the Genetic and Evolutionary Computation Conference Companion*. (ACM), (2017).
 71. M Emmons-Bell, et al., Regenerative adaptation to electrochemical perturbation in planaria: A molecular analysis of physiological plasticity. *iScience* **22**, 147–165 (2019).
 72. S Kauffman, C Peterson, B Samuelsson, C Troein, Genetic networks with canalizing boolean rules are always stable. *Proc. Natl. Acad. Sci.* **101**, 17102–17107 (2004).
 73. WL Shew, H Yang, S Yu, R Roy, D Plenz, Information capacity and transmission are maximized in balanced cortical networks with neuronal avalanches. *J. Neurosci.* **31**, 55–63 (2011).
 74. N Bertschinger, T Natschläger, Real-time computation at the edge of chaos in recurrent neural networks. *Neural Comput.* **16**, 1413–1436 (2004).
 75. P Råmö, S Kauffman, J Kesseli, O Yli-Harja, Measures for information propagation in boolean networks. *Phys. D: Nonlinear Phenom.* **227**, 100–104 (2007).
 76. T Mora, W Bialek, Are biological systems poised at criticality? *J. Stat. Phys.* **144**, 268–302 (2011).
 77. IC Fiebelkorn, S Kastner, A rhythmic theory of attention. *Trends Cogn. Sci.* **23**, 87–101 (2019).
 78. NL Golding, NP Staff, N Spruston, Dendritic spikes as a mechanism for cooperative long-term potentiation. *Nature* **418**, 326–331 (2002).
 79. IC Fiebelkorn, YB Saalmann, S Kastner, Rhythmic sampling within and between objects despite sustained attention at a cued location. *Curr. Biol.* **23**, 2553–2558 (2013).
 80. M Kirchhoff, T Parr, E Palacios, K Friston, J Kiverstein, The markov blankets of life: autonomy, active inference and the free energy principle. *J. The Royal Soc. Interface* **15**, 20170792 (2018).
 81. M Lungarella, O Sporns, Information self-structuring: key principle for learning and development in *Proc. of the 4th Int. Conf. on Development and Learning*. (IEEE), pp. 25–30 (2005).
 82. K Friston, C Thornton, A Clark, Free-energy minimization and the dark-room problem. *Front. Psychol.* **3** (2012).
 83. J Bruineberg, E Rietveld, Self-organization, free energy minimization, and optimal grip on a field of affordances. *Front. Hum. Neurosci.* **8** (2014).
 84. RK Logan, What is information?: Why is it relativistic and what is its relationship to materiality, meaning and organization. *Information* **3**, 68–91 (2012).
 85. DJ Nicholson, Is the cell really a machine? *J. Theor. Biol.* **477**, 108–126 (2019).
 86. R Pfeifer, M Lungarella, F Iida, Self-organization, embodiment, and biologically inspired robotics. *Science* **318**, 1088–1093 (2007).
 87. M Merleau-Ponty, *The Structure of Behavior*. (Duchesne University Press), (1983).
 88. J Bongard, R Pfeifer, *How the Body Shapes the Way We Think*. (MIT Press, Cambridge, Massachusetts), (2006).
 89. N Wiener, *Cybernetics or Control and Communication in the Animal and the Machine*. (MIT press), (1948).
 90. G Pezzulo, M Levin, Top-down models in biology: explanation and control of complex living systems above the molecular level. *J. The Royal Soc. Interface* **13**, 20160555 (2016).
 91. O Sporns, Selectionist and instructionist ideas in neuroscience in *International Review of Neurobiology*. (Elsevier), pp. 3–26 (1994).
 92. D Ha, J Schmidhuber, Recurrent world models facilitate policy evolution in *Advances in Neural Information Processing Systems 31*. (Curran Associates, Inc.), pp. 2451–2463 (2018) <https://worldmodels.github.io>.
 93. MD Egbert, XE Barandiaran, EAD Paolo, A minimal model of metabolism-based chemotaxis. *PLoS Comput. Biol.* **6**, e1001004 (2010).
 94. KO Stanley, DB D’Ambrosio, J Gauci, A hypercube-based encoding for evolving large-scale neural networks. *Artif. Life* **15**, 185–212 (2009).
 95. G Buzsáki, Neuronal oscillations in cortical networks. *Science* **304**, 1926–1929 (2004).
 96. D Zenklusen, DR Larson, RH Singer, Single-RNA counting reveals alternative modes of gene expression in yeast. *Nat. Struct. & Mol. Biol.* **15**, 1263–1271 (2008).
 97. SP MacEvoy, TD Hanks, MA Paradiso, Macaque v1 activity during natural vision: Effects of natural scenes and saccades. *J. Neurophysiol.* **99**, 460–472 (2008).
 98. C Rajkai, et al., Transient cortical excitation at the onset of visual fixation. *Cereb. Cortex* **18**, 200–209 (2007).
 99. ZF Mainen, TJ Sejnowski, Influence of dendritic structure on firing pattern in model neocortical neurons. *Nature* **382**, 363–366 (1996).
 100. A Paré, et al., Visualization of individual scr mRNAs during drosophila embryogenesis yields evidence for transcriptional bursting. *Curr. Biol.* **19**, 2037–2042 (2009).
 101. A Raj, CS Peskin, D Tranchina, DY Vargas, S Tyagi, Stochastic mRNA synthesis in mammalian cells. *PLoS Biol.* **4**, e309 (2006).
 102. L Cai, N Friedman, XS Xie, Stochastic protein expression in individual cells at the single molecule level. *Nature* **440**, 358–362 (2006).
 103. RD Kamm, et al., Perspective: The promise of multi-cellular engineered living systems. *APL Bioeng.* **2**, 040901 (2018).
 104. S Kriegman, D Blackiston, M Levin, J Bongard, A scalable pipeline for designing reconfigurable organisms. *Proc. Natl. Acad. Sci.* **117**, 1853–1859 (2020).
 105. H Lipson, JB Pollack, Automatic design and manufacture of robotic lifeforms. *Nature* **406**, 974–978 (2000).
 106. CT Mueller, JA Ochsendorf, Combining structural performance and designer preferences in evolutionary design space exploration. *Autom. Constr.* **52**, 70–82 (2015).
 107. S Kriegman, Ph.D. thesis (University of Vermont) (2020).
 108. L van der Maaten, G Hinton, Visualizing data using t-sne. *J. Mach. Learn. Res.* **9**, 2579–2605 (2008).

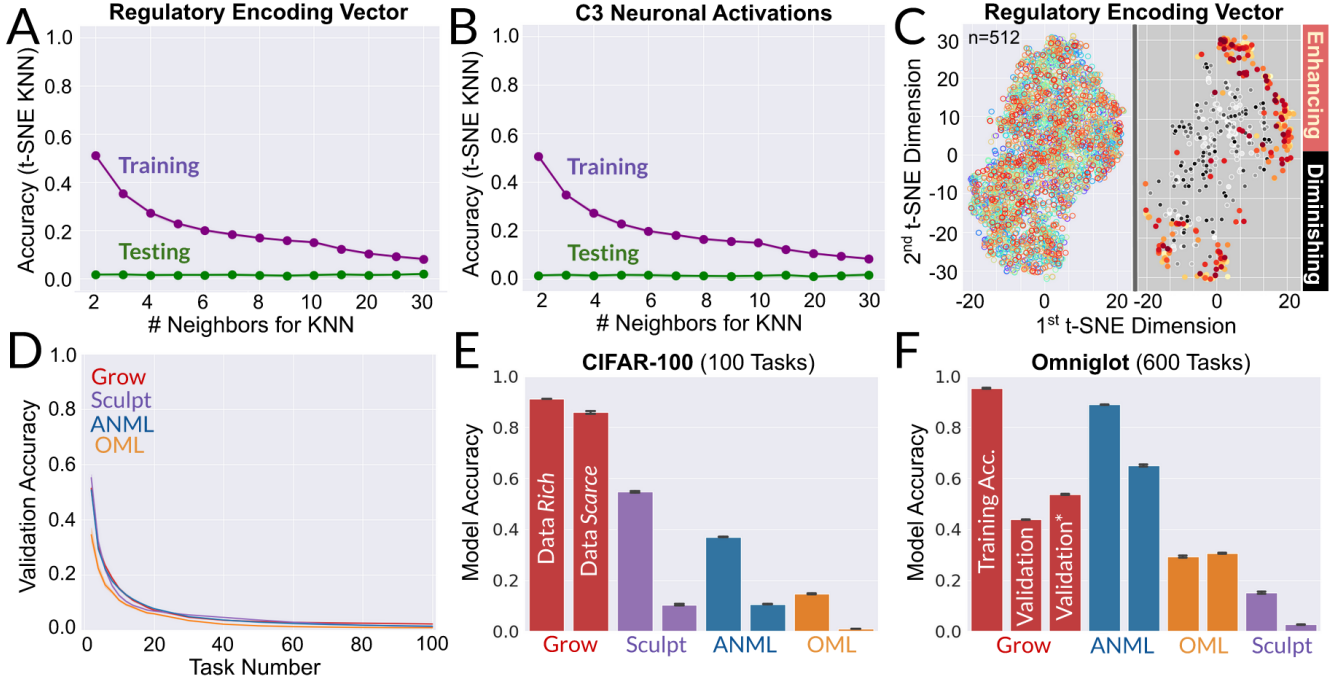


Fig. 5. (A) Dimensionally reduced regulatory encoding vectors are not identifiable by their class ID. Following dimensional reduction ($D=2$) through a combination of PCA (50 components) and t-SNE (108), K-Nearest Neighbors for class prediction was performed. These results show that images belonging to a particular class are not represented by the regulator in a way that is more similar than images belonging to other classes. If they were, class prediction accuracy by KNN clustering would be high. Confidence intervals report standard deviation across all runs ($n=25$). **(B)** Representations in the classifier are not identifiable by their class ID. Results that are virtually identical to (A) obtain for KNN clustering of representations produced by the third convolutional layer of the classifier. Thus, images that belong to a given class are not represented by the classifier in a way that is more similar than representations of images belonging to other classes. Confidence intervals report standard deviation across all runs ($n=25$). **(C)** The regulator toggles between two states, each with a similar presentation across tasks (*enhancing* and *diminishing*). Points in the right panel are dimensionally reduced regulator encodings (Fig. 1A, “encoding”) for the images that are the most enhancing (top 256, yellow-red) and most diminishing (bottom 256, grey-black). Coloring by task identity (left panel) yields no discernable clusters, and for no run are tasks identifiable by their t-SNE projections using K-Nearest Neighbors (SI Appendix, Fig.S1). Dimensional reduction is obtained through a combination of principle component analysis (50 components) and the t-SNE algorithm (108). **(D)** Validation accuracy under domain transfer to ImageNet is low for all models. For comparison, Grow trained in the IID setting (epochs=1) on the same data is virtually indistinguishable from the online setting reported here, with a relative decline in test accuracy of 0.01% ($p\text{-value}=0.36$). However, increasing the number of epochs from 1 to 3 in the IID setting has a negligible effect on performance. This is to be expected, as generalization on complex problems has historically been achieved by multiple rounds of IID training. Given the capacity to generalize to unseen images from the same domain used for meta-learning (F), this does not signify an inability of our model to generalize. Rather, it reflects the difficulty of generalizing under domain transfer from few images learned sequentially. **(E)** Training accuracy under domain transfer to CIFAR-100. **Rich:** Grow=91.1% \pm 0.56% (SD), Sculpt=54.7% \pm 2.4%, ANML=37% \pm 1.70%, OML=14.6% \pm 2.6%. **Scarce:** Grow=85.9% \pm 5.12%, Sculpt=10.4% \pm 2.9%, ANML=10.57% \pm 0.73%, OML=1% \pm 0.10%. Accuracy for 600 previously unseen tasks learned sequentially from Omniglot. **Training:** Grow=95.2% \pm 1.4%, Sculpt=15.1% \pm 2.23%, ANML=88.9% \pm 0.59%, OML=29.3% \pm 2.23%. **Validation:** Grow=43.82% \pm 0.93%, Sculpt=2.6% \pm 0.28%, ANML=65.06% \pm 2.88%, OML=30.6% \pm 1.04%. It is worth reiterating that in ANML only the final layer of the classification network is trainable. When the regulatory output layers that flow to C1, C2, and C3 in Grow are fixed, but the weights they govern are trainable, validation accuracy (“Grow”, 3rd bar) increases to 53.75% \pm 1.45%. This final version of Grow corresponds to a relative drop of 15.5% compared to the IID setting (epochs=3: 63.5%). By comparison, Sculpt forgets catastrophically on this 600-task problem in the online setting, and in the IID setting it performs approximately the same as IID Grow (epochs=3: 63.1%, $p\text{-value}=6.1 \times 10^{-7}$). These results show that Grow can generalize in the online setting, but that this ability is limited when the stream of inputs is either highly complex or falls outside of the native meta-learning distribution. However, the capacity for generalization is not the focus of the present study.

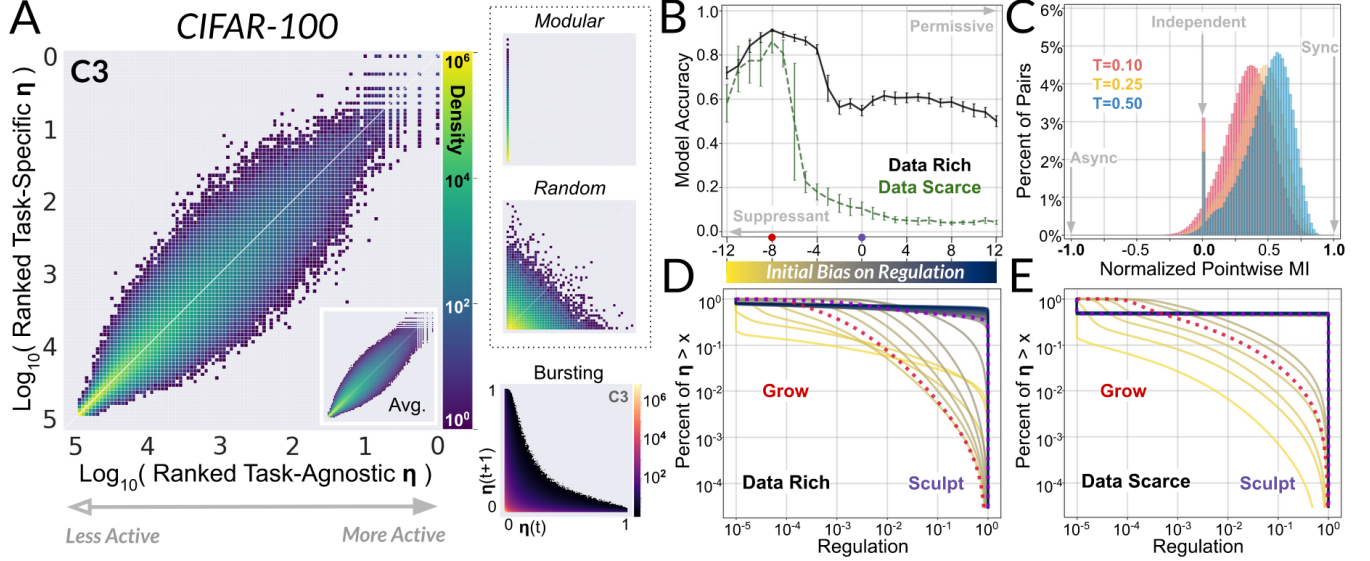


Fig. 6. Regulation under domain transfer to CIFAR-100 does not elicit task-specific modularity. Instead, the most active weights over a given task are the most active weights over all tasks, and no synapse dramatically changes rank for any individual task (*synaptic recycling*). For each task, regulatory signals are ranked according to their Task-Specific activity (Eq.1) and Task-Agnostic activity (Eq.2). Ranked lists are then transformed to a logarithmic scale (5=least active, 0=most active) and used to fill a two-dimensional histogram with 100 bins per dimension (1000 cells in total). The final matrix is filled with data from all 100 tasks for a single run and colored by density on a logarithmic scale (67). The inset reports the average over all runs, with outlier cells of density=1 in less than 25% of runs removed. For individual runs, see Fig.S11 (Rich) and Fig.S16 (Scarce). *Synthetic Rankings*: as a conceptual aid, we provide synthetic versions of (A) that report what would be (i) “perfect” task-specific modularity and (ii) Gaussian random regulation. For regulation that is perfectly task *Modular*, weights are randomly sorted into 100 disjoint subsets and assigned (i) a random and constant regulatory signal for the task their subset ID corresponds to, and (ii) a value of 0 for every other task, thus producing synthetic task-specific modules. For regulation that is *Random*, weights are assigned a Gaussian random regulatory signal for all inputs. *Bursting* (non-synthetic): we observe that highly permissive regulation at time t is predictive of suppressant regulation at time $t + 1$. Thus, synaptic recruitment is highly transient (*synaptic bursting*). Time-lagged regulatory outputs under domain transfer are plotted over all runs by stacking two-dimensional histograms for the 75th-99th percentiles of regulation ranked by task-agnostic mean. Lower percentiles are almost uniformly suppressant, and so are omitted from this figure. We then plot the average density over the stack of all runs. Outlier cells that have a density less than or equal to 1 post-stacking are masked. Results for individual runs without masking or stacking are presented in (SI Appendix, Fig.S3). (B) Meta-learned regulation that is initialized to be more permissive is less successful under domain transfer than meta-learned regulation that is initialized to be more suppressant. We report the final performance under domain transfer to ImageNet for the range of meta-learning biases on regulation covering the range (-12, 12). For each initial bias not equal to 0 (Sculpt) or -8 (Grow), 10 independent models were meta-trained and evaluated under domain transfer over 25 separate runs (250 total runs per treatment). (C) Bursting synapses exhibit a positive bias in their degree of correlation, but very few synapses are strongly synchronized, indicating relatively heterogeneous spike compositions. Each color represents a different threshold (T) for which a synapse is said to burst if it receives regulation above that threshold, resulting in a binary sequence of length 3000 for each synapse per run ($N=25$). Normalized point-wise mutual information (68) is then computed for each pair of synapses having firing rate > 1% under each threshold for all runs. (D,E) For data rich (D) and data scarce (E) meta-learning, regulators that are increasingly successful under domain transfer exhibit regulatory distributions that are increasingly linear (scale-free) in the logarithmic CCDF. This trend holds across several orders of magnitude in all convolutional layers of the Grow condition (SI Appendix, Fig.23), and thus reveals regulation to be approximately scale-free (54). However, our conclusion does not hinge on whether regulation is precisely power-law distributed, or merely log-normally distributed. These results show that sensor *growth* obtains a *proportional* balance of activity and suppression that is analogous to the balance of order and disorder in critical systems at the edge of chaos (69), while sensor *sculpting* does not. We present CCDF plots for the highest performing models for each treatment.

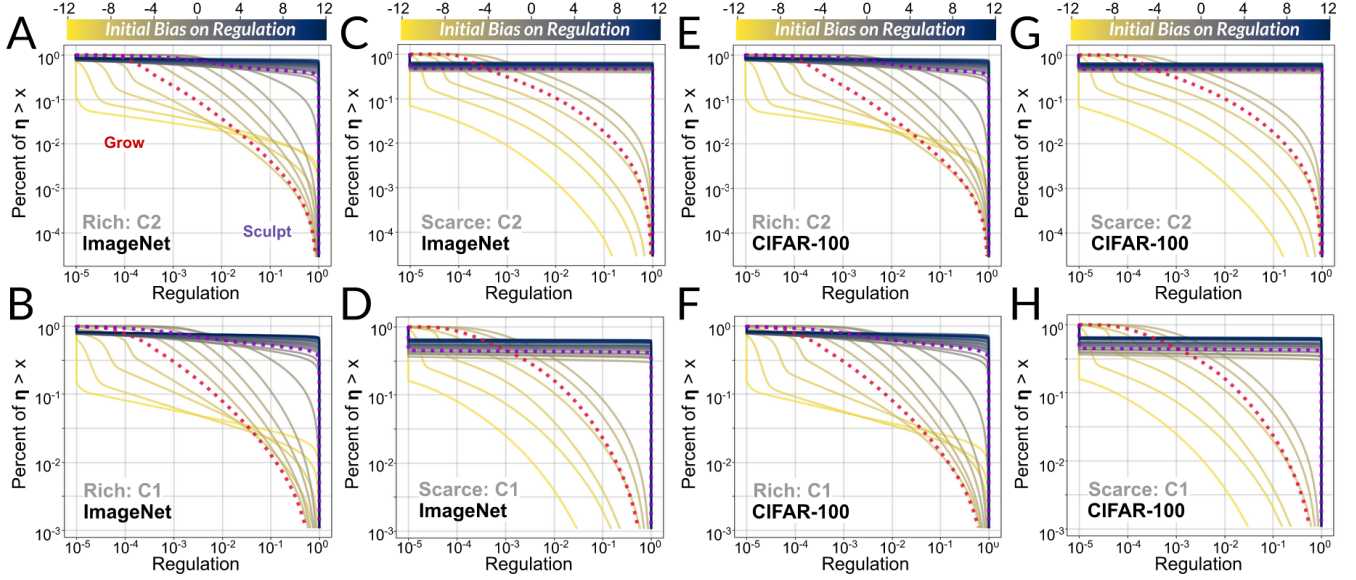


Fig. 7. A-H For data rich and data scarce meta-learning, regulators that are increasingly successful under domain transfer exhibit regulatory distributions that are increasingly linear (scale-free) in the logarithmic CCDF. This trend holds across several orders of magnitude in all convolutional layers of the Grow condition, and thus reveals regulation to be approximately scale-free (54). However, our results do not hinge on whether regulation is precisely power-law distributed, or merely log-normally distributed. These results shows that Grow has obtained a proportional balance of activity and suppression that is analogous to the balance of order and disorder in critical systems at the edge of chaos (69). We present CCDF plots for the highest performing runs for each model.

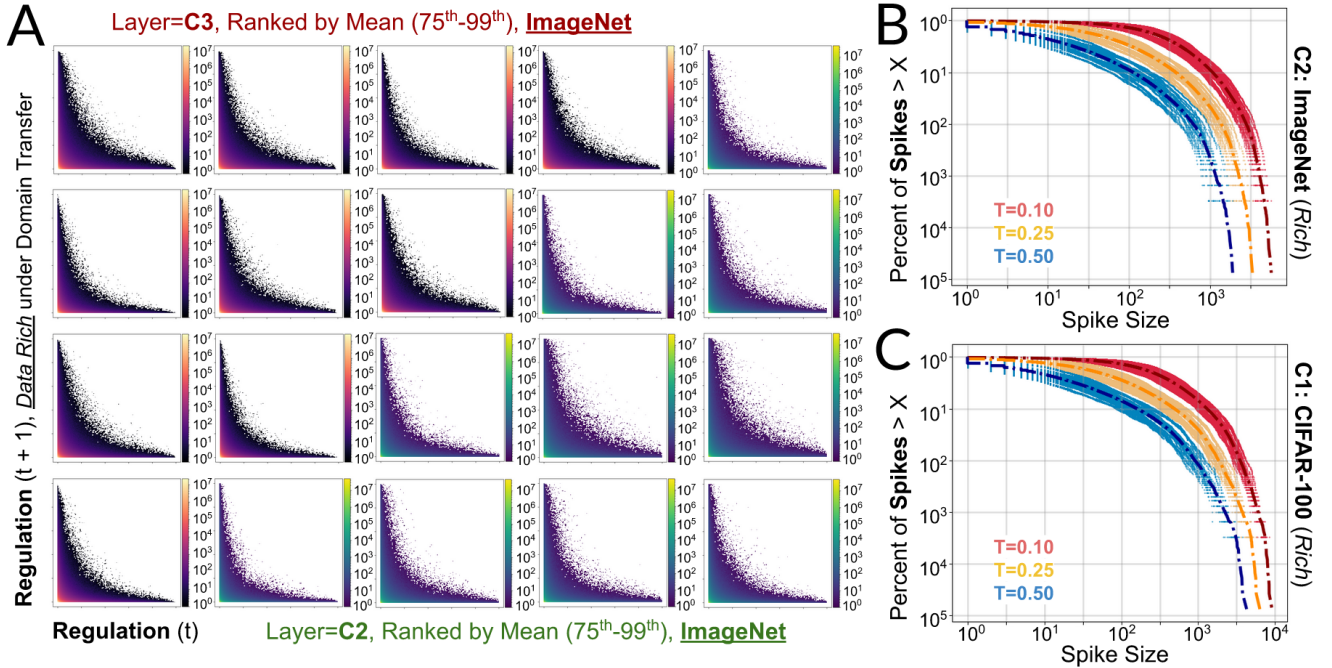


Fig. 8. (A) Regulation in the data rich condition under domain transfer to ImageNet induces sparse synaptic bursting, which is characterized by highly transient activity in a subset of weights in response to particular *images* rather than particular *tasks*. For synapses that are not uniformly suppressed (for layers C3, C2), the most likely state for a synapse at time $t+1$ that gets activated at time t is inactivation. Plots are generated using a 2D histogram having 250 bins uniformly spaced between 0 and 1. Cells are colored on a logarithmic scale by density. Results for C3 and C2 are presented for synapses receiving regulation that ranks in the 75th to 99th percentile by task-agnostic mean. We find minor differences between layers in their degree of transience. **(B, C)** Regulation is calibrated to control the *amount* of sensory processing in the classifier, rather than the *task-modular location* where such processing occurs. Increasingly large spikes, which induce greater sensory processing, are correspondingly rare, resulting in heavy-tailed distribution as shown by the logarithmic complementary cumulative distribution function (CCDF)

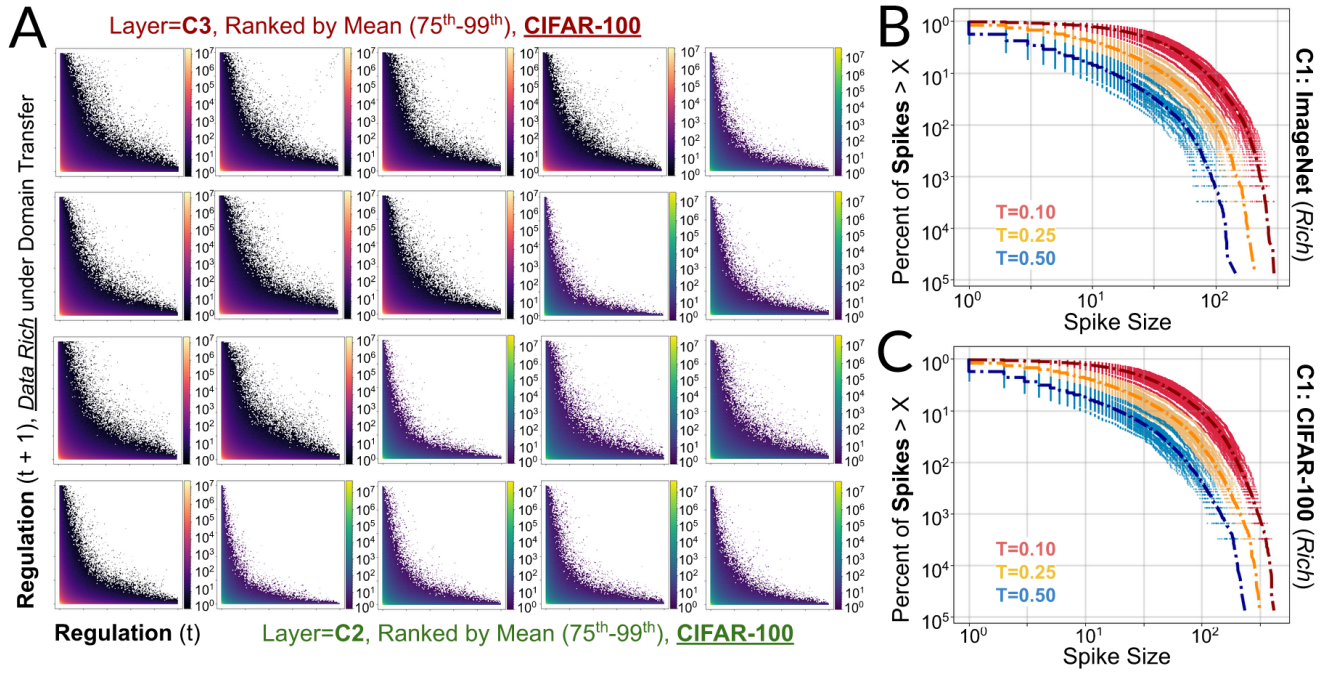


Fig. 9. Regulation in the data rich condition under domain transfer to CIFAR-100 induces sparse synaptic bursting, which is characterized by highly transient activity in a subset of weights in response to particular *images* rather than particular *tasks*. For synapses that are not uniformly suppressed (for layers C3, C2), the most likely state for a synapse at time $t+1$ that gets activated at time t is inactivation. Plots are generated using a 2D histogram having 250 bins uniformly spaced between 0 and 1. Cells are colored on a logarithmic scale by density. Results for C3 and C2 are presented for synapses receiving regulation that ranks in the 75th to 99th percentile by task-agnostic mean. We find minor differences between layers in their degree of transience. **(B, C)** Regulation is calibrated to control the *amount* of sensory processing in the classifier, rather than the task-modular *location* where such processing occurs. Increasingly large spikes, which induce greater sensory processing, are correspondingly rare, resulting in heavy-tailed distribution as shown by the logarithmic complementary cumulative distribution function (CCDF)

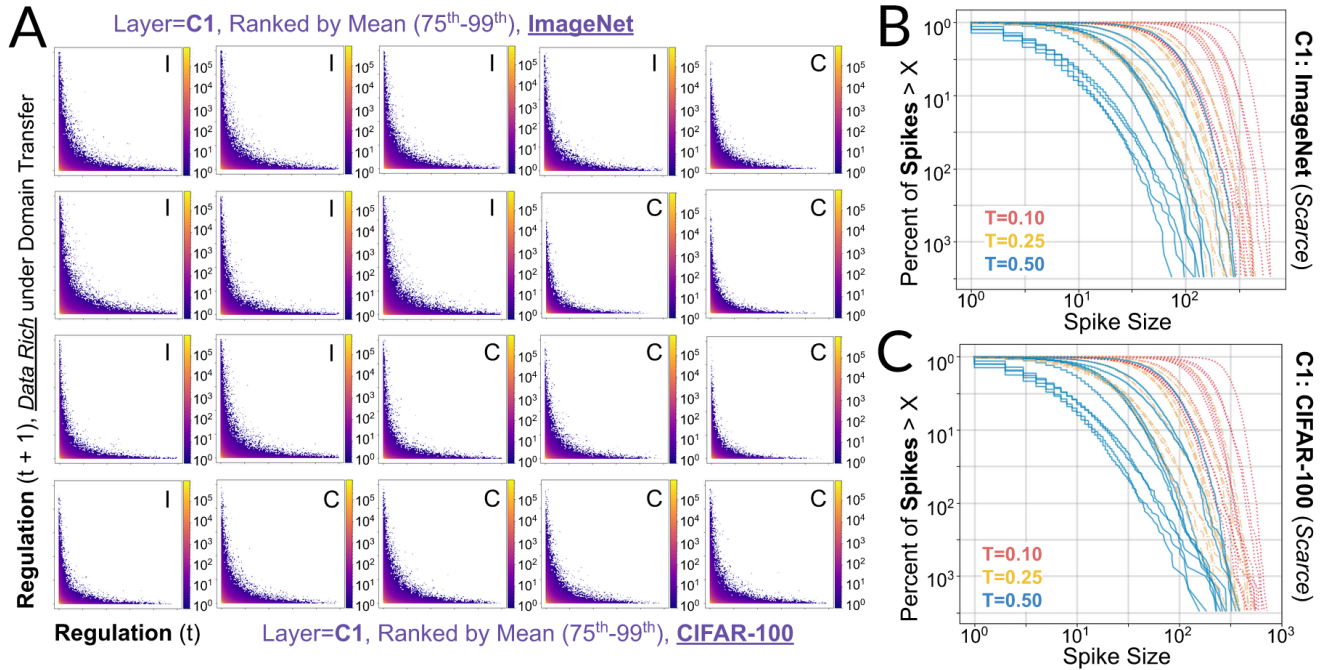


Fig. 10. Regulation in the data rich condition under domain transfer to ImageNet and CIFAR-100 induces sparse synaptic bursting, which is characterized by highly transient activity in a subset of weights in response to particular *images* rather than particular *tasks*. For synapses that are not uniformly suppressed (for layer C1), the most likely state for a synapse at time $t+1$ that gets activated at time t is inactivation. Plots are generated using a 2D histogram having 250 bins uniformly spaced between 0 and 1. Cells are colored on a logarithmic scale by density. Results for C1 are presented for synapses receiving regulation that ranks in the 75th to 99th percentile by task-agnostic mean. We find minor differences between layers in their degree of transience. **(B, C)** Regulation is calibrated to control the *amount* of sensory processing in the classifier, rather than the task-modular *location* where such processing occurs. Increasingly large spikes, which induce greater sensory processing, are correspondingly rare, resulting in heavy-tailed distribution as shown by the logarithmic complementary cumulative distribution function (CCDF)

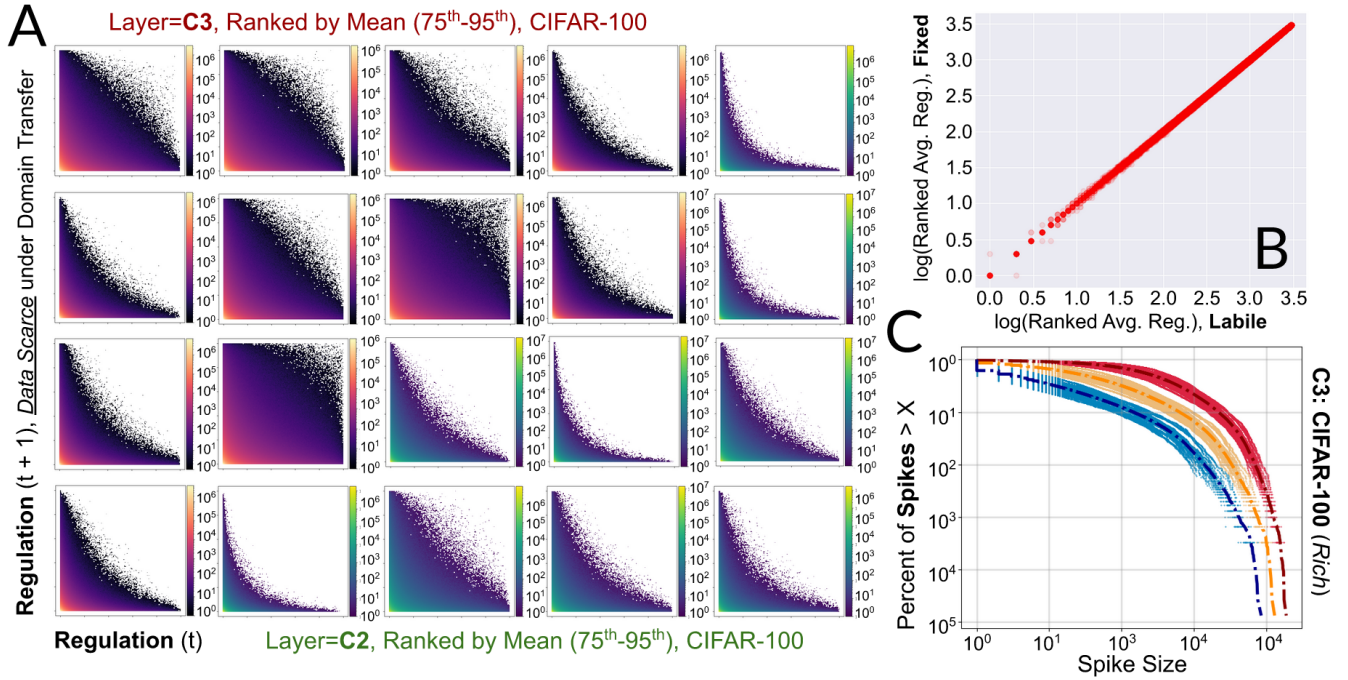


Fig. 11. Regulation in the data scarce condition under domain transfer to ImageNet induces sparse synaptic bursting, which is characterized by highly transient activity in a subset of weights in response to particular *images* rather than particular *tasks*. For synapses that are not uniformly suppressed (in layer C3, C2), the most likely state for a synapse at time $t+1$ that gets activated at time t is inactivation. Plots are generated using a 2D histogram having 250 bins uniformly spaced between 0 and 1. Cells are colored on a logarithmic scale by density. Results for C3 and C2 are presented for synapses receiving regulation that ranks in the 75th to 95th percentile by task-agnostic mean. We find minor differences between layers in their degree of transience. **(B)** Mean regulation elicited by a given image is virtually identical when the regulatory output layers to C3 are trainable compared to when they are fixed under domain transfer to ImageNet. Thus, images can be roughly classified as either "intrinsically" enhancing or diminishing. We plot results for all outputs over 25 independent runs. **(C)** Regulation is calibrated to control the *amount* of sensory processing in the classifier, rather than the task-modular *location* where such processing occurs. Increasingly large spikes, which induce greater sensory processing, are correspondingly rare, resulting in heavy-tailed distribution as shown by the logarithmic complementary cumulative distribution function (CCDF). This pattern is observed for all convolutional layers in the classifier (SI Appendix, Fig.S3, Fig.S4, Fig.S5). Each color in this figure corresponds to a different threshold (T) for which a synapse is said to burst if it receives regulation above that threshold. Results were obtained for 25 independent runs.

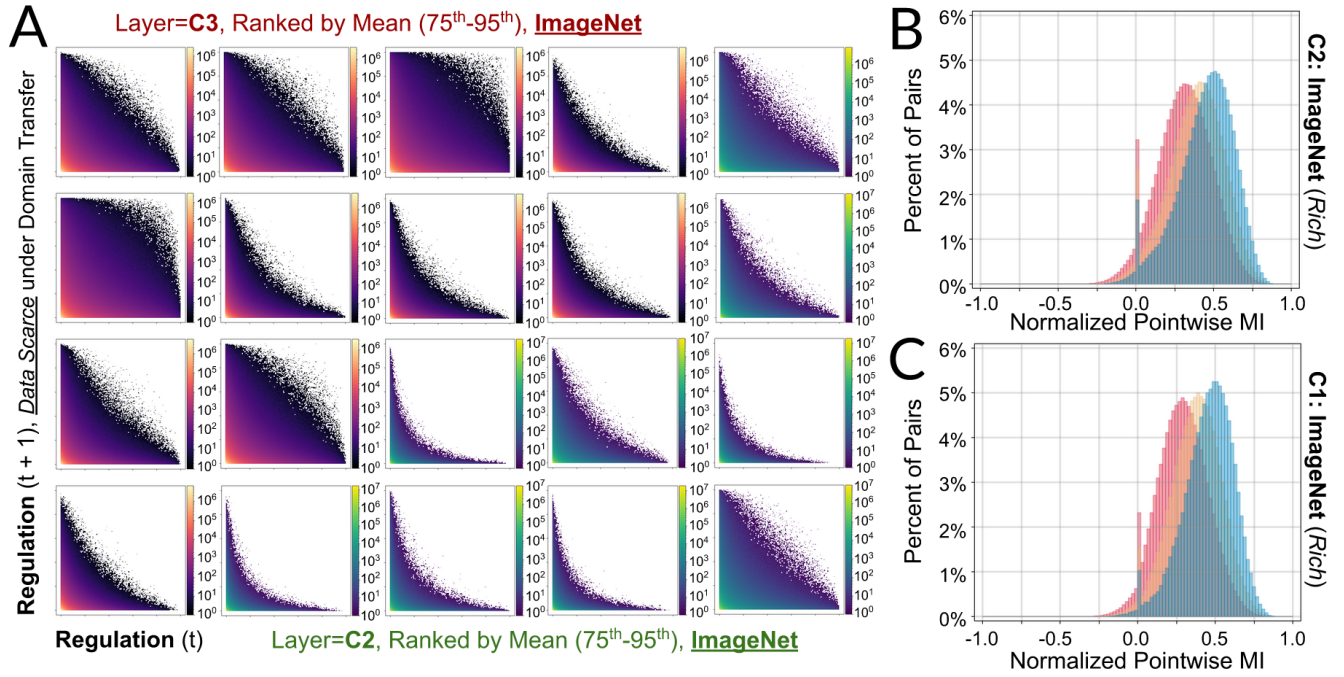


Fig. 12. Regulation in the data scarce condition under domain transfer to CIFAR-100 induces sparse synaptic bursting, which is characterized by highly transient activity in a subset of weights in response to particular *images* rather than particular *tasks*. For synapses that are not uniformly suppressed (for layers C3, C2), the most likely state for a synapse at time $t+1$ that gets activated at time t is inactivation. However, we find that synaptic bursting in the data scarce condition is less sparse than the data rich condition. Plots are generated using a 2D histogram having 250 bins uniformly spaced between 0 and 1. Cells are colored on a logarithmic scale by density. Results for C3 and C2 are presented for synapses receiving regulation that ranks in the 75th to 95th percentile by task-agnostic mean. We find minor differences between layers in their degree of transience. **(B)** Strongly correlated bursting in pairs of synapses within layer C2 is rare, indicating variable spike composition. **(C)** Correlated bursting in pairs of synapses within layer C1 is also rare.

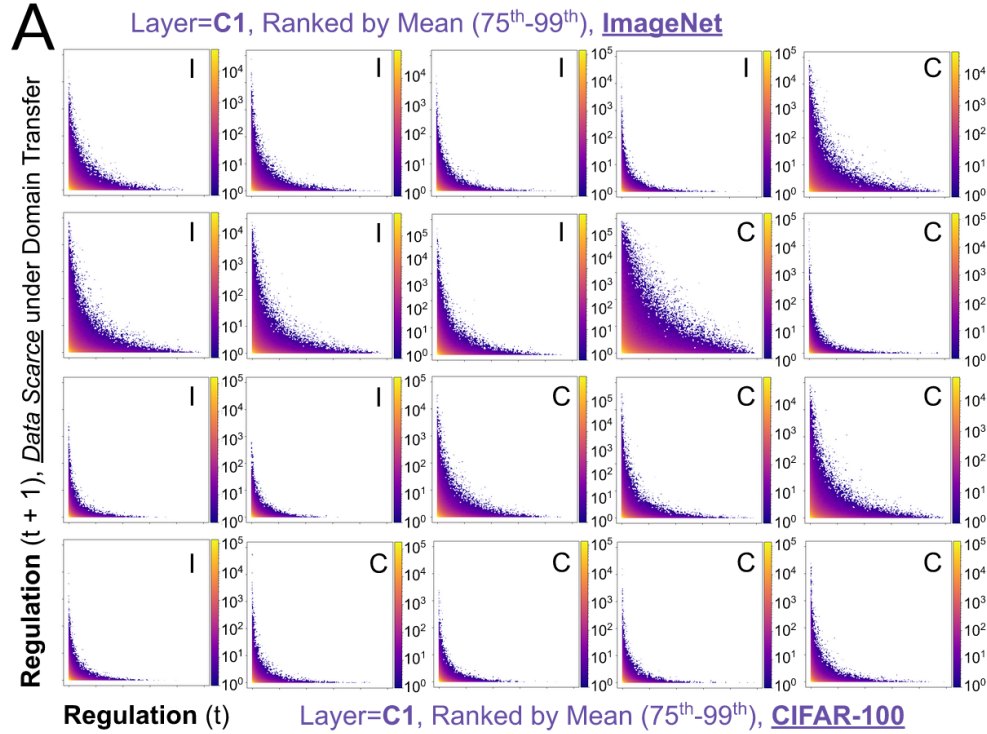


Fig. 13. Regulation in the data scarce condition under domain transfer to ImageNet and CIFAR-100 induces sparse synaptic bursting, which is characterized by highly transient activity in a subset of weights in response to particular *images* rather than particular *tasks*. For synapses that are not uniformly suppressed (for layer C1), the most likely state for a synapse at time $t+1$ that gets activated at time t is inactivation. Plots are generated using a 2D histogram having 250 bins uniformly spaced between 0 and 1. Cells are colored on a logarithmic scale by density. Results for C1 are presented for synapses receiving regulation that ranks in the 75th to 99th percentile by task-agnostic mean.

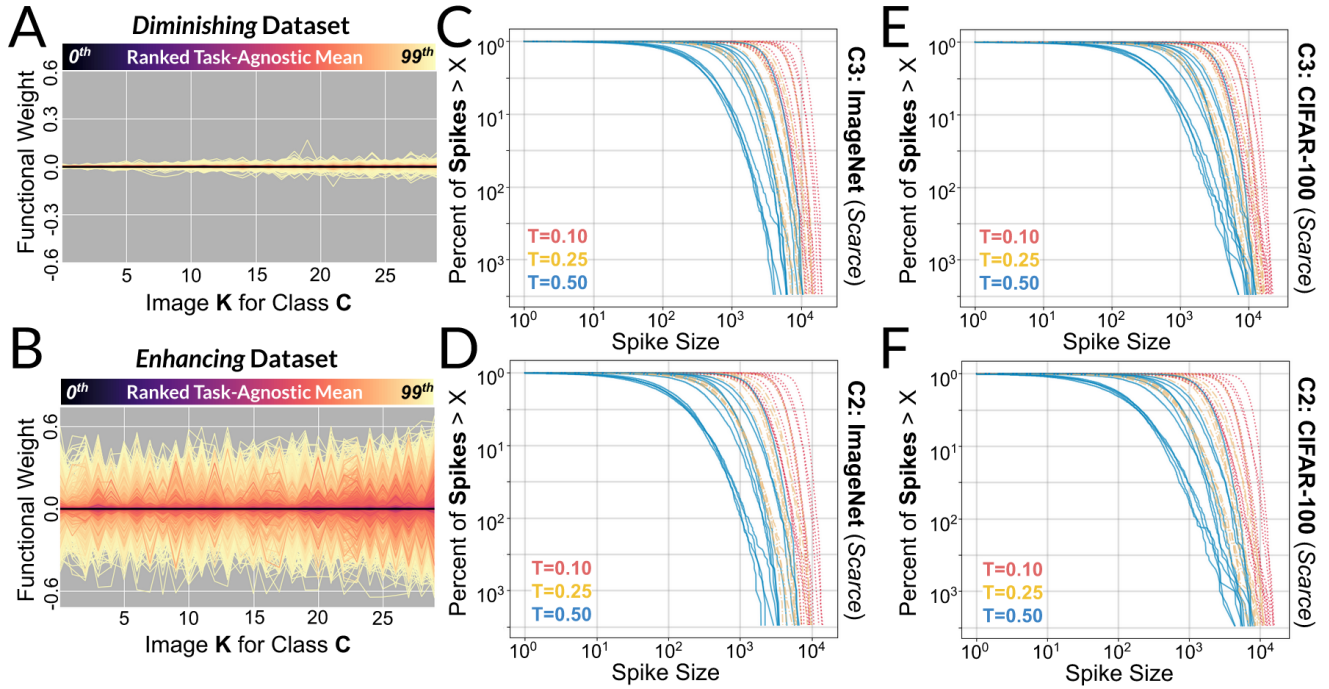


Fig. 14. (A) Images from the diminishing dataset result in diminished sensory processing in the classifier. We plot functional weights in C3 over a randomly sampled task window for a randomly sampled run. Functional weights are defined as synaptic values post-regulatory gating, and are colored by centile according to ranked mean computed over all domain transfer tasks. (B) Images from the enhancing dataset result in enhanced sensory processing in the classifier. We plot functional weights in C3 over a randomly sampled task window for a randomly sampled run. Functional weights are defined as synaptic values post-regulatory gating, and are colored by centile according to ranked mean computed over all domain transfer tasks. (C,D,E,F) Regulation (data scarce) is calibrated to control the *amount* of sensory processing in the classifier, rather than the task-modular *location* where such processing occurs. Increasingly large spikes, which induce greater sensory processing, are correspondingly rare, resulting in heavy-tailed distribution as shown by the logarithmic complementary cumulative distribution function (CCDF)

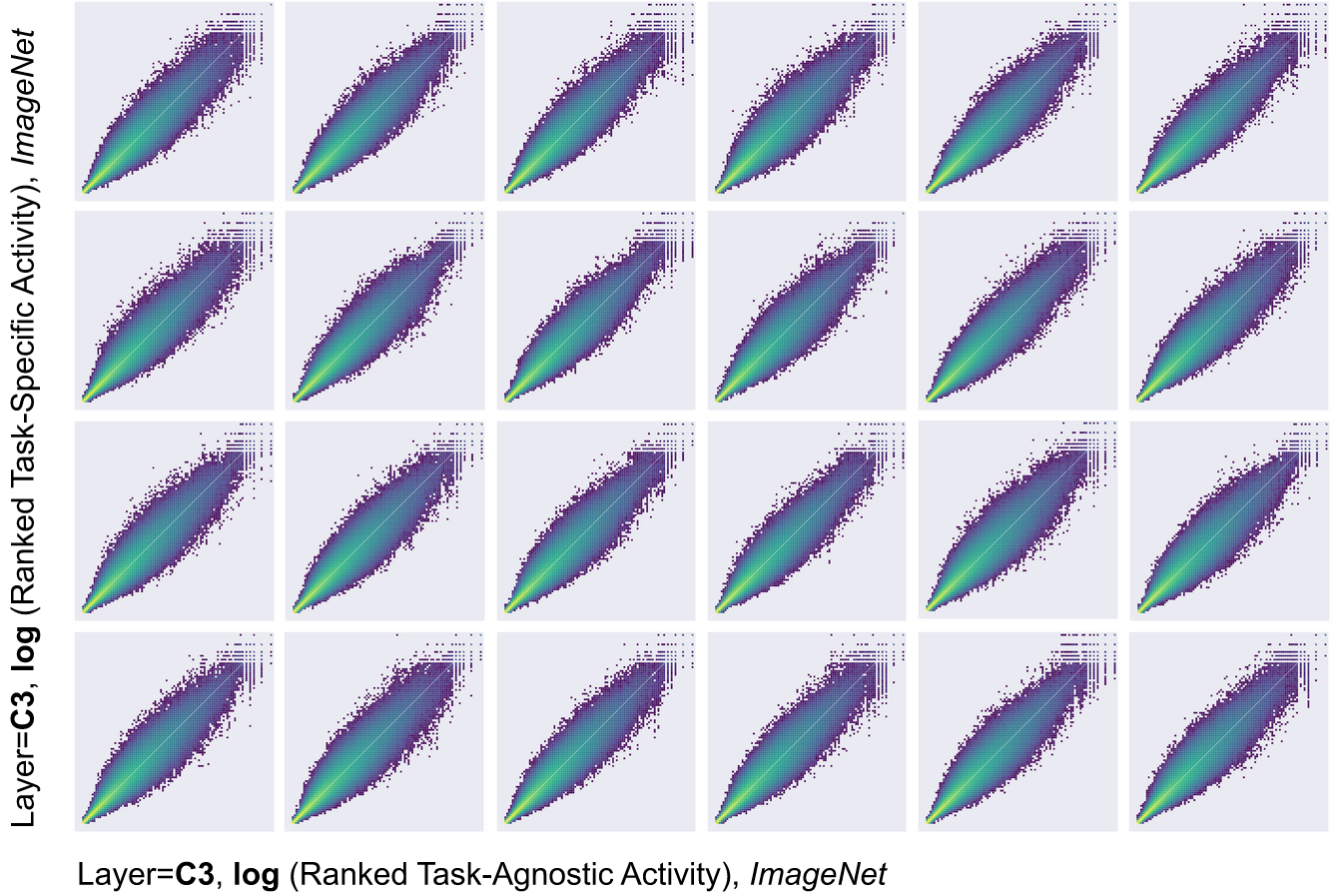


Fig. 15. Regulation in C3 of the data rich condition under domain transfer to ImageNet does not elicit task-specific modularity. Instead, the most active weights on a given task are the most active weights over all tasks (*synaptic recycling*), and no synapse dramatically changes rank for any individual task. See Fig.S2, and Figure 3 in the main text, for details regarding figure construction. Here we present results for a single trial for each of the remaining 24 models. Finally, we note that the degree of context *sensitivity* is higher for layer C3 under domain transfer to ImageNet and CIFAR-100 than it is for layers C2 and C1. This is distinct from context *modularity*, and likely reflects the commonly observed property that downstream layers are dedicated to less generic features of the input.

Layer=C3, \log (Ranked Task-Specific Activity), CIFAR-100



Layer=C3, \log (Ranked Task-Agnostic Activity), CIFAR-100

Fig. 16. Regulation in C3 of the data rich condition under domain transfer to CIFAR-100 does not elicit task-specific modularity. Instead, the most active weights on a given task are the most active weights over all tasks (*synaptic recycling*), and no synapse dramatically changes rank for any individual task. See Fig.S2, and Figure 3 in the main text, for details regarding figure construction. Here we present results for a single trial for the remaining 24 independent models. Finally, we note that the degree of context *sensitivity* is higher for layer C3 under domain transfer to ImageNet and CIFAR-100 than it is for layers C2 and C1. This is distinct from context *modularity*, and likely reflects the commonly observed property that downstream layers are dedicated to less generic features of the input.

Layer=C2, \log (Ranked Task-Specific Activity), ImageNet



Layer=C2, \log (Ranked Task-Agnostic Activity), ImageNet

Fig. 17. Regulation in C2 of the data rich condition under domain transfer to ImageNet does not elicit task-specific modularity. Instead, the most active weights on a given task are the most active weights over all tasks (*synaptic recycling*), and no synapse dramatically changes rank for any individual task. See Fig.S2, and Figure 3 in the main text, for details regarding figure construction. Here we present results for a single trial for 24 independent models. Compared to results for regulation of C3 under domain transfer to ImageNet, regulation of C2 is noticeably less context-sensitive. This may be attributed to the common observation that successive layers in neural networks attend to decreasingly generic properties of inputs. Nevertheless, context-dependent modules, which are an extreme form of context sensitivity, are not present in any of the convolutional layers.

Layer=C2, \log (Ranked Task-Specific Activity), CIFAR-100



Layer=C2, \log (Ranked Task-Agnostic Activity), CIFAR-100

Fig. 18. Regulation in C2 of the data rich condition under domain transfer to CIFAR-100 does not elicit task-specific modularity. Instead, the most active weights on a given task are the most active weights over all tasks (*synaptic recycling*), and no synapse dramatically changes rank for any individual task. See Fig.S2, and Figure 3 in the main text, for details regarding figure construction. Here we present results for a single trial for each of the remaining 24 models. Compared to results for regulation of C3 under domain transfer to CIFAR-100, regulation of C2 is noticeably less context-sensitive. This may be attributed to the common observation that successive layers in neural networks attend to decreasingly generic properties of inputs. Nevertheless, context-dependent modules, which are an extreme form of context sensitivity, are not present in any of the convolutional layers.

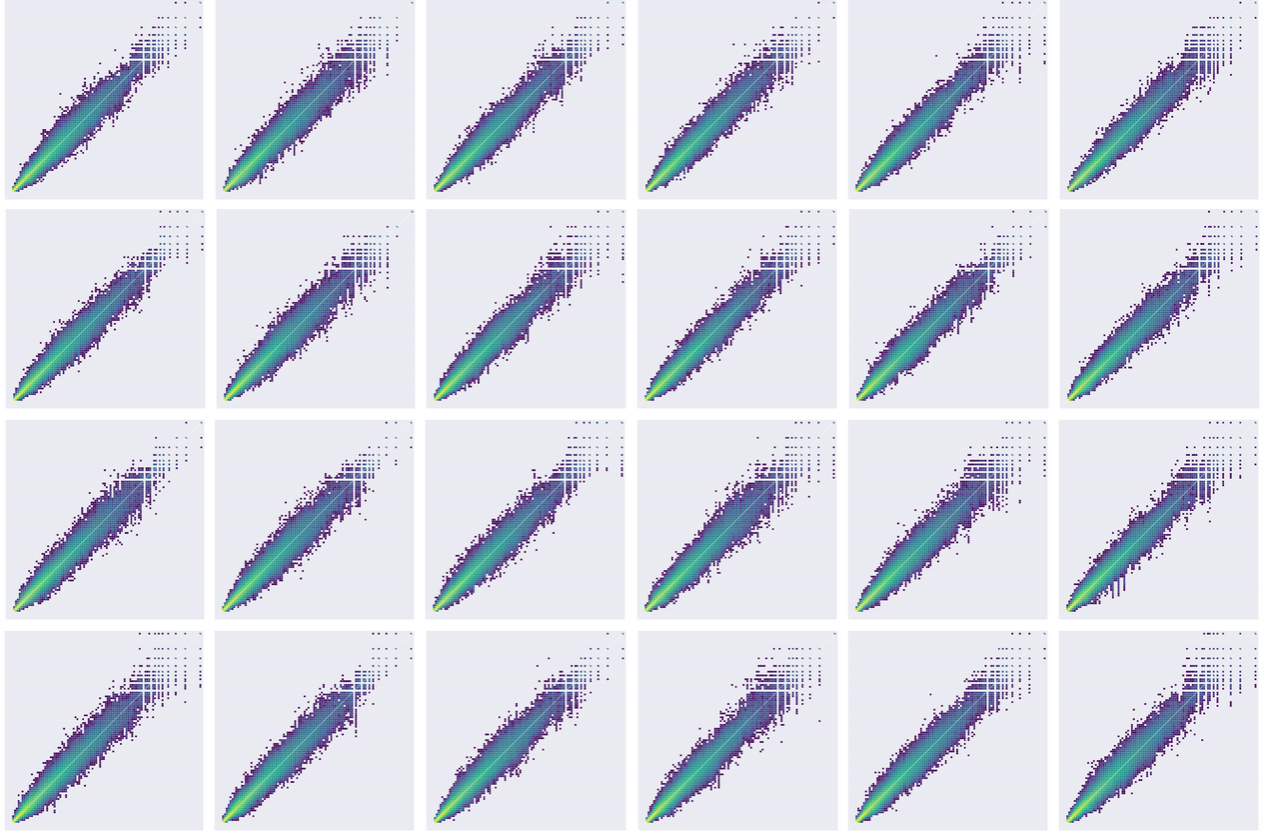
Layer=C1, \log (Ranked Task-Specific Activity), ImageNet



Layer=C1, \log (Ranked Task-Agnostic Activity), ImageNet

Fig. 19. Regulation in C1 of the data rich condition under domain transfer to ImageNet does not elicit task-specific modularity. Instead, the most active weights on a given task are the most active weights over all tasks (*synaptic recycling*), and no synapse dramatically changes rank for any individual task. See Fig.S2, and Figure 3 in the main text, for details regarding figure construction. Here we present results for a single trial for each of the remaining 24 models. Compared to results for regulation of C3 and C2 under domain transfer to ImageNet, regulation of C1 is noticeably less context-sensitive. This may be attributed to the common observation that successive layers in neural networks attend to decreasingly generic properties of inputs. Nevertheless, context-dependent modules, which are an extreme form of context sensitivity, are not present in any of the convolutional layers of the classifier.

Layer=C1, \log (Ranked Task-Specific Activity), CIFAR-100



Layer=C1, \log (Ranked Task-Agnostic Activity), CIFAR-100

Fig. 20. Regulation in C1 of the data rich condition under domain transfer to CIFAR-100 does not elicit task-specific modularity. Instead, the most active weights on a given task are the most active weights over all tasks (*synaptic recycling*), and no synapse dramatically changes rank for any individual task. See Fig.S2, and Figure 3 in the main text, for details regarding figure construction. Here we present results for a single trial for each of the remaining 24 models. Compared to results for regulation of C3 and C2 under domain transfer to CIFAR-100, regulation of C1 is noticeably less context-sensitive. This may be attributed to the common observation that successive layers in neural networks attend to decreasingly generic properties of inputs. Nevertheless, context-dependent modules, which are an extreme form of context sensitivity, are not present in any of the convolutional layers of the classifier.

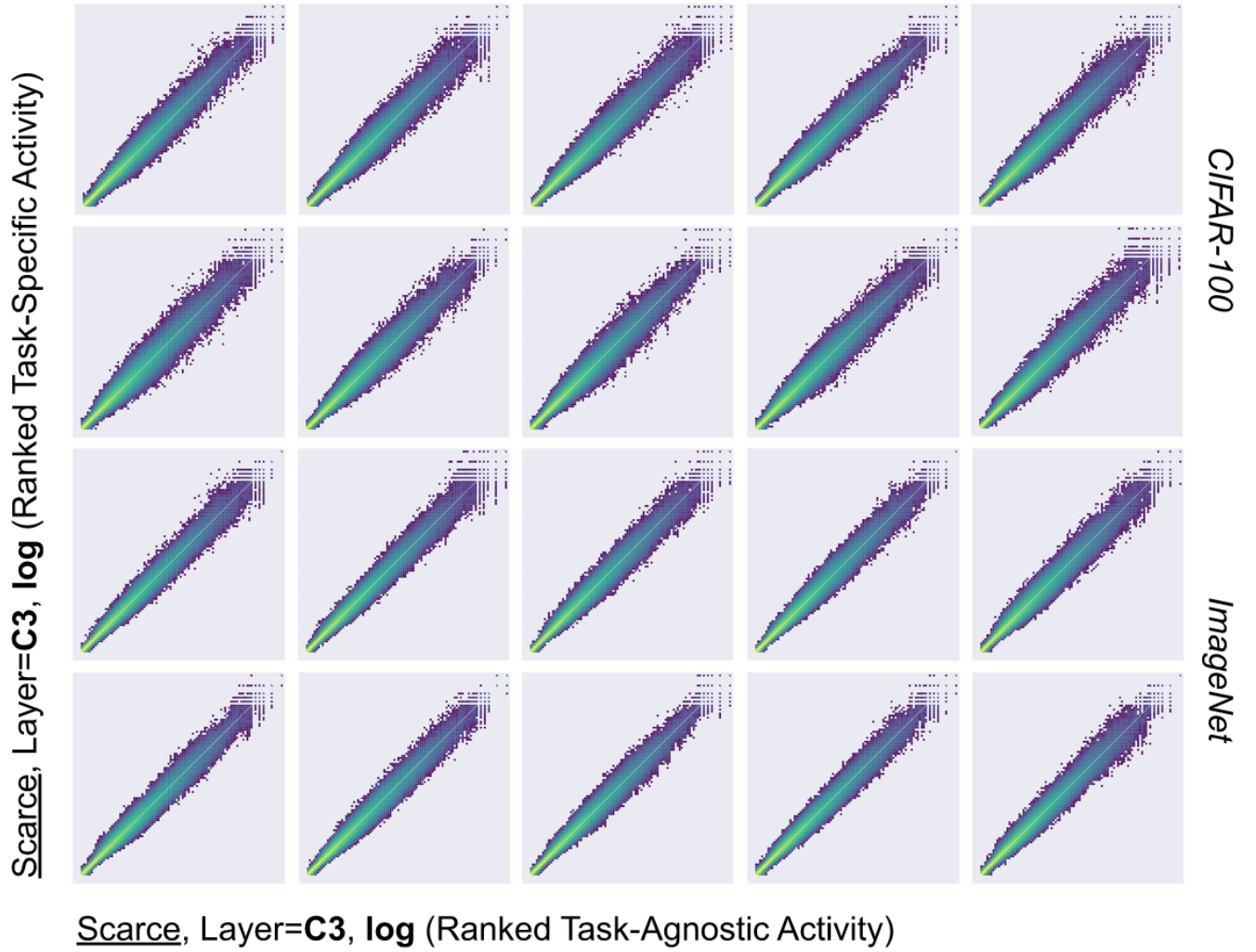


Fig. 21. The lack of task-specific modularity observed in the regulation of C3 in the data rich condition is recapitulated in regulation of C3 in the data scarce condition. We also find that regulation in the data scarce condition is noticeably less context sensitive than in the data rich condition. Thus, we find that synaptic recycling in C3 is more strongly pronounced in the data scarce condition. We present results for 10 randomly sampled independent runs per dataset.

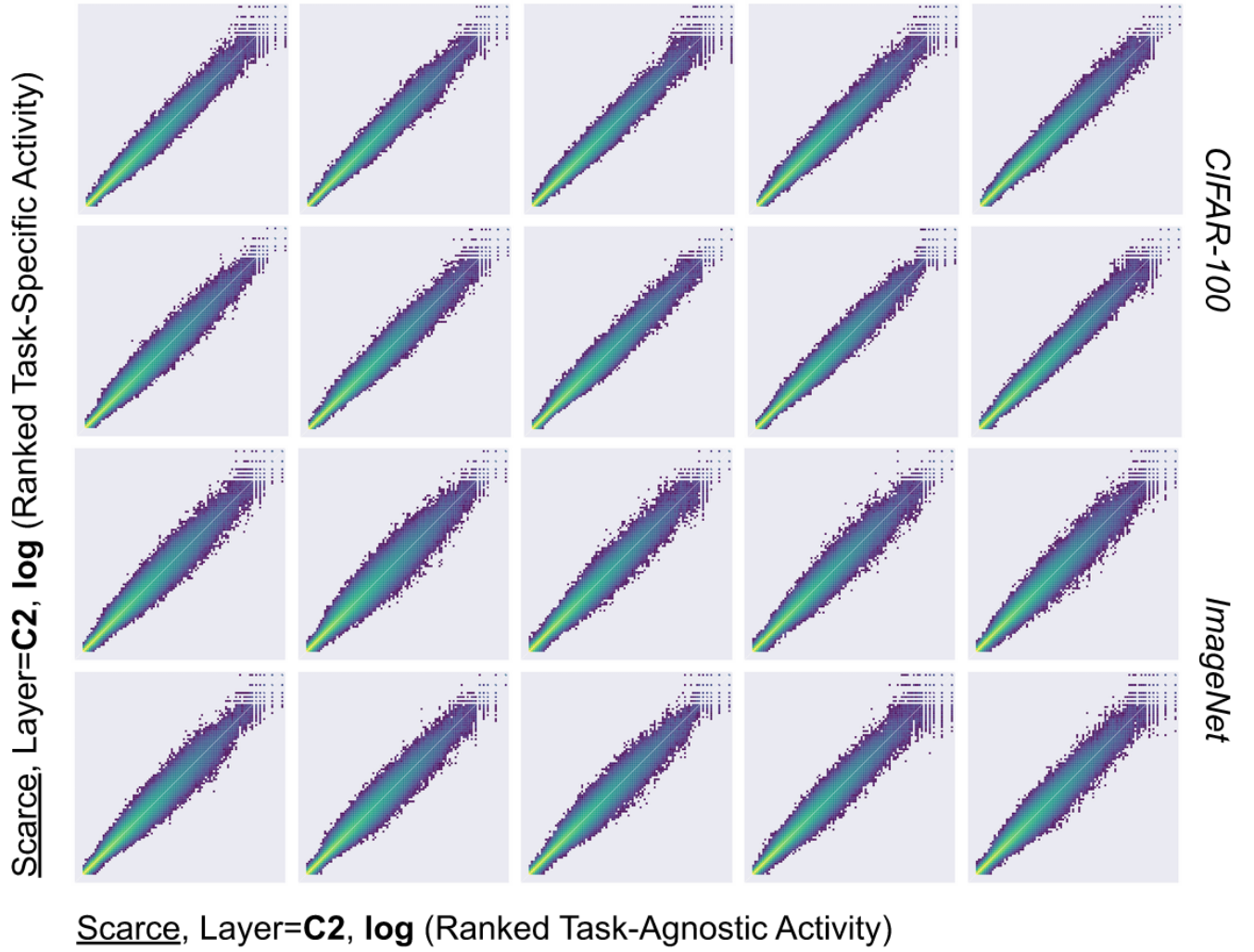


Fig. 22. The lack of task-specific modularity observed in the regulation of C2 in the data rich condition is recapitulated in regulation of C2 in the data scarce condition. We also find that regulation in the data scarce condition is noticeably less context sensitive than in the data rich condition. Thus, we find that synaptic recycling in C2 is more strongly pronounced in the data scarce condition. We present results for 10 randomly sampled independent runs per dataset.

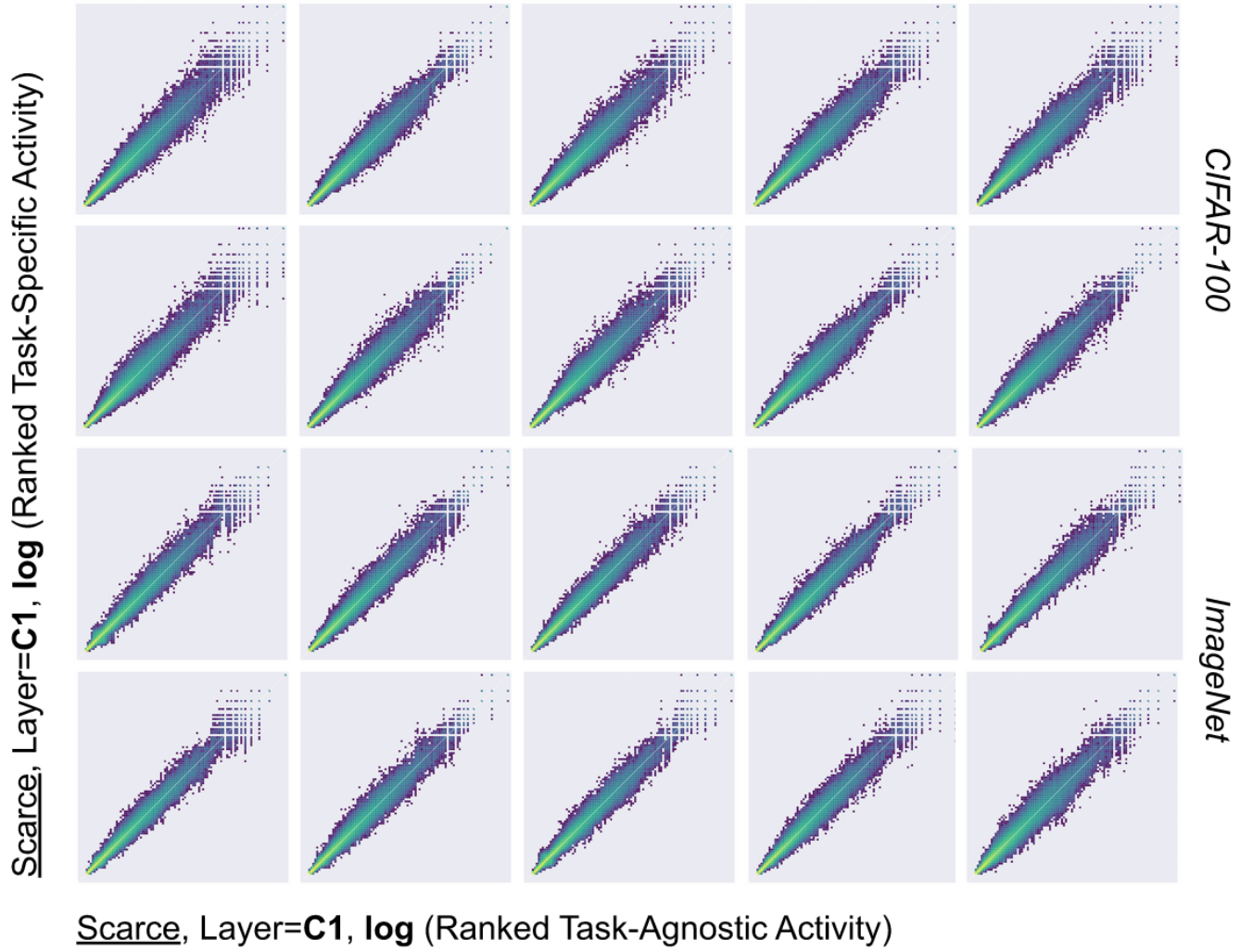


Fig. 23. The lack of task-specific modularity observed in the regulation of C1 in the data rich condition is recapitulated in regulation of C1 in the data scarce condition. We also find that regulation in the data scarce condition is noticeably less context sensitive than in the data rich condition. Thus, we find that synaptic recycling in C1 is more strongly pronounced in the data scarce condition. We present results for 10 randomly sampled independent runs per dataset.